nature biomedical engineering

ARTICLES

https://doi.org/10.1038/s41551-021-00780-3

Check for updates

# Amelioration of post-traumatic osteoarthritis via nanoparticle depots delivering small interfering RNA to damaged cartilage

Sean K. Bedingfield[1], Juan M. Colazo[1], Fang Yu[1], Danielle D. Liu[1], Meredith A. Jackson[1], Lauren E. Himmel[2], Hongsik Cho[3,4], Leslie J. Crofford[2,5], Karen A. Hasty[3,4] and Craig L. Duvall[1]✉

**The progression of osteoarthritis is associated with inflammation triggered by the enzymatic degradation of extracellular matrix in injured cartilage. Here we show that a locally injected depot of nanoparticles functionalized with an antibody targeting type II collagen and carrying small interfering RNA targeting the matrix metalloproteinase 13 gene (*Mmp13*), which breaks down type II collagen, substantially reduced the expression of MMP13 and protected cartilage integrity and overall joint structure in acute and severe mouse models of post-traumatic osteoarthritis. MMP13 inhibition suppressed clusters of genes associated with tissue restructuring, angiogenesis, innate immune responses and proteolysis. We also show that intra-articular injections of the nanoparticles led to greater reductions in disease progression than either a single injection or weekly injections of the steroid methylprednisolone. Sustained drug retention by targeting collagen in the damaged extracellular matrix of osteoarthritic cartilage may also be an effective strategy for the treatment of osteoarthritis with other disease-modifying drugs.**

Osteoarthritis (OA) is a chronic degenerative disease of the entire joint that leads to pain and loss of mobility, resulting in diminished quality of life. OA is caused by a complex interplay between mechanical and biochemical factors[1]. Some well-established risk factors include poor joint alignment or injury[2], obesity[3], genetic disposition[4] and aging[5]. Multiple signalling molecules are known to be central to OA pathogenesis, such as interleukin-1β (IL-1β), Wnt, Jun N-terminal kinase (JNK) and reactive oxygen species (ROS)[1,6,7]. These signalling pathways converge independently toward increased production of matrix metalloproteinases (MMPs), a step of critical importance in cartilage degradation and progression of OA symptoms[1].

Post-traumatic OA (PTOA) is a form of OA induced by a mechanical joint injury. Common injuries include ligament and meniscal tears, cartilage damage, bone fractures from high-impact landings and dislocations. These injuries are particularly common among young athletes and military personnel and result in an accelerated pathology, requiring surgical intervention 7–9 years earlier on average than standard OA[8]. Although PTOA accounts for only 12% of all cases of OA in the United States, it comes at a greater cost and loss of quality-adjusted life years (QALYs) due to its earlier and more accelerated onset[9]. PTOA-initiating injuries mechanically disturb the extracellular matrix (ECM) and stimulate synoviocytes and chondrocytes to produce inflammatory cytokines and MMPs[10]. MMPs are key enzymes in OA-related cartilage ECM destruction that degrade the critical structural components of cartilage, including type II collagen (Col2). Degradation of Col2 and other ECM components destroys the chondrocyte niche. Released ECM degradation by-products also have pro-inflammatory signalling properties[1,11] that trigger a degenerative cycle that perpetuates until the cartilage is fully destroyed. Because patients with joint injuries are highly predisposed to developing PTOA, there is potential for early therapeutic intervention to block disease onset or progression at an early stage.

Current pharmaceutical management of OA is solely palliative, and there are no clinically approved disease-modifying OA drugs (DMOADs). There are five corticosteroids that have been approved by the US Food and Drug Agency for intra-articular OA therapy, but these therapies provide only temporary pain relief. Steroids do not target the underlying cause of the disease and are not recommended for long-term management[12], as they have been shown to actually cause loss of cartilage volume[13] (when given 4 times per year for 2 years), have been shown to increase the risk of requiring joint replacement[14] and are associated with chondrotoxicity[15]. MMP13 is a key proteolytic driver of cartilage loss in OA, as indicated by reduced surgically induced OA progression in MMP13-knockout mice and in wild-type mice treated with broad MMP inhibitors[16]. Clinical trials on small molecule MMP inhibitors (tested mostly for cancer treatment) have been suspended due to pain associated with musculoskeletal syndrome, which is believed to be linked to systemic delivery of small molecules that non-selectively inhibit multiple MMPs—some of which (MMP2, 3, 4, 7 and 9) are involved in normal tissue homeostasis[17–19]. Production of MMP13-selective small molecule inhibitors is complicated by shared domains of the collagenases and the homology of the catalytic site[20]. One tested MMP13 inhibitor, PF152, reduced severity of lesions in a canine PTOA model[21], but also caused nephrotoxicity[22] through off-target effects on the human organic anion transporter 3. For these reasons, we hypothesize that selectively targeting *Mmp13* (which has not been associated with musculoskeletal syndrome) through delivery of a locally retained RNA interference (RNAi) therapy could be an effective and safe approach for blocking the degenerative PTOA process following joint injury.

[1]Department of Biomedical Engineering, Vanderbilt University, Nashville, TN, USA. [2]Department of Pathology, Microbiology and Immunology, Vanderbilt University Medical Center, Nashville, TN, USA. [3]Department of Orthopaedic Surgery and Biomedical Engineering, University of Tennessee Health Science Center-Campbell Clinic, Memphis, TN, USA. [4]Department of Veterans Affairs Medical Center, Memphis, TN, USA. [5]Department of Medicine, Division of Rheumatology and Immunology, Vanderbilt University Medical Center, Nashville, TN, USA. ✉e-mail: craig.duvall@vanderbilt.edu

Intra-articular injections are used clinically for OA, but face unique drug delivery challenges. One of the major barriers is that synovial fluid is continuously exchanged in the joint, causing most drugs to be cleared rapidly into the lymphatic system[23,24]. The synovial vasculature clears small molecules, whereas the lymphatics drain away macromolecules[25,26], resulting in joint half-lives ranging from 1 h to 4 h for commonly used steroids[24]. These challenges leave an unmet need for OA therapies that are better retained within the joint after local injection. Targeting of nanoscale particles is one promising approach that has traditionally relied on using chondroitin sulfate, Col2-binding peptides and bisphosphonates[27–29]. Chondroitin sulfate and Col2-binding peptides anchor particles to the cartilage matrix and reduce convective transport through synovial fluid flow, whereas bisphosphonates can be used to bind to subchondral bone that may be exposed in advanced OA disease. ECM bioadhesion has been minimally utilized for delivery of small molecules and, to our knowledge, its use has not been investigated for local retention of biologics with intracellular targets[30].

In this study, we sought to anchor *Mmp13* RNAi nanoparticles to sites of early cartilage damage in OA and to confirm that matrix targeting can provide functional benefits for delivery of intracellular-acting biologics. RNAi is critical in this application because short interfering RNA (siRNA) can be designed to have selective complementarity with MMP13 mRNA, obviating the concerns about enzyme selectivity associated with small molecule inhibitors. The clinical utility of siRNA medicines is supported by the recent clinical trial success and US Food and Drug Agency approval of Onpattro (patisiran) for treatment of hereditary transthyretin-mediated amyloidosis and Givlaari (givosiran) for acute hepatic porphyria[31,32]. Here we extended the use of polymeric siRNA nanoparticle complexes (siNPs)[33–36] to develop a form of this carrier that binds to sites of early OA cartilage damage using a Col2 monoclonal antibody (mAbCII) (E4-D4 clone; Supplementary Fig. 1). This antibody clone recognizes an epitope of cyanogen bromide (CNBr) peptide 10 and has been proven to be cross-reactive with Col2 from multiple species (mouse, human, pig, bovine and guinea pig) but not with type 1 collagen. The antibody epitope becomes more accessible when other proteins or proteoglycans in the cartilage matrix are lost. Previous studies show that cartilage Col2 is more exposed and accessible for binding after injury[37] and that the mAbCII antibody can be used as a targeted nano-diagnostic molecule for intravital measurement of the severity of OA[38]. We formulated and therapeutically tested mAbCII-functionalized siNPs (mAbCII-siNPs) as a locally injectable system that creates an in situ depot of *Mmp13* RNAi nanomedicine in PTOA-afflicted joints (Fig. 1a). Matrix-targeted delivery of an intracellular-acting biologic such as siRNA represents a strategic departure from the convention of targeting internalizing cellular receptors. We validate the utility of this approach and demonstrate its therapeutic potential as a DMOAD in a model of mechanical PTOA.

## Results and discussion

The mAbCII-siNPs comprise an endosome-escaping, RNA-condensing core and a passivating, colloidally stabilizing poly (ethylene glycol) (PEG) surface amenable to antibody conjugation. The diblock co-polymer that constitutes the siNPs was synthesized through reversible addition–fragmentation chain transfer (RAFT) polymerization of a random co-polymer of 50 mol% 2-(dimethylamino)ethyl methacrylate (DMAEMA) and 50 mol% butyl methacrylate (BMA) from a carboxy-PEG-4-cyano-4-(ethylsulfanylthio carbonyl)sulfanylpentanoic acid (ECT) macro-chain transfer agent (macro-CTA) and verified by NMR (Supplementary Fig. 2). The poly(DMAEMA-co-BMA) (DB) random co-polymer block has a balance of hydrophobic BMA and cationic DMAEMA monomers that has been finely tuned to drive nanoparticle (NP) self-assembly and stabilization (using BMA), enable electrostatic siRNA packaging (using DMAEMA), and have an appropriate p*K*a and level of hydrophobicity that drives pH-dependent membrane-disruptive function in the pH range of the early endosome[33,39–41]. The Col2-targeting mAbCII was conjugated to COOH-PEG-ECT using *N*-hydroxysulfosuccinimide; 1-ethyl-3-(3-(dimethylamino)propyl) carbodiimide (sNHS/EDC) chemistry (Fig. 1b). Successful conjugation of PEG-*bl*-DB to mAbCII was validated by fast protein liquid chromatography (FPLC; Supplementary Fig. 1d), and the resultant polymers were formulated into siNPs by complexation with siRNA at pH 4 followed by raising to physiologic pH (Fig. 1c). The control groups included siNPs with no antibody conjugation (bare-siNPs) and siNPs functionalized with a control off-target antibody (mAbCtrl-siNPs). 'Dual hydrophobization' was also used in all siNP formulations. This approach combines the hydrophobicity of BMA in the core of the siNP with C16 modification of the siRNA through conjugation to palmitic acid to improve siNP stability and duration of gene silencing[35,42].

**Chemico-physical in vitro characterization of mAbCII-siNPs.** The underlying siNP that was developed here in a mAbCII-functionalized format has been previously characterized[33,36,39,42]. These studies have consistently shown a hydrodynamic diameter of approximately 100 nm and approximately neutral zeta potential due to the PEG (or, in some formats, zwitterionic siNP surface forming polymer block). The in vivo circulation half-life after intravenous injection[33] is approximately 20 min. These siNPs are cytocompatible in vitro[33] and can be tolerated upon repeated, intravenous administration in vivo, with minimal histologic or immunologic consequences[42].

The hydrodynamic diameter, siRNA encapsulation efficiency, pH-dependent membrane-disruptive behaviour (as an indirect indicator of endosome escape), and cell viability were assayed for mAbCII-siNPs compared to non-targeted siNPs. These characteristics of the mAbCII-siNPs were not statistically different from those of the non-functionalized siNPs in these assays (Fig. 2a–d). The mAbCII-siNPs, prepared at a 1:40 antibody:polymer ratio for optimized cartilage binding (Fig. 2f), had an average hydrodynamic diameter of 124 nm with a polydispersity index of 1.1, as determined by dynamic light scattering (Fig. 2a). Encapsulation of siRNA was efficient (about 80%) at ratios of positively charged nitrogen groups ($N^+$) in polymer side chains to negatively charged phosphodiester groups ($P^-$) ($N^+$:$P^-$ ratios) of 10 or above (Fig. 2b). The haemolysis assay demonstrated significant membrane lysis at the pH of early endosome (6.8) and below, and negligible activity at extracellular pH (7.4) (Fig. 2c). Cell viability was approximately 80% or greater for doses of up to 150 nM (Fig. 2d).

Silencing of *Mmp13* was tested in cultured mouse chondrogenic ATDC5 cells stimulated with TNF. The cells were pre-treated for 24 h with the siRNA formulations, stimulated with 20 ng ml$^{-1}$ TNF for 24 h, and then assayed for *Mmp13* gene expression using TaqMan quantitative PCR with reverse transcription (RT–qPCR). The sequences that were screened to identify the leading *Mmp13* siRNA are listed in Supplementary Table 1 and Supplementary Fig. 3. The best candidate (siMMP13) demonstrated more than 80% knockdown of *Mmp13* expression with a 50 nM dose delivered by the mAbCII-siNPs when compared with a nontargeting siRNA sequence (siNEG) (Fig. 2e). These data show that siNP bioactivity is maintained following antibody conjugation and that the mAbCII-siNPs can achieve potent *Mmp13* silencing in cells under pro-inflammatory conditions.

**Ex vivo Col2 targeting and substrate-mediated RNAi in ATDC5 cells.** The mAbCII-siNPs were assessed for binding to porcine cartilage explants that were pre-treated with trypsin, which initiates formation of lesions of the articular surface, similar to those seen in OA[43]. Trypsin does not damage the triple helical structure of Col2 but rather removes the telopeptide ends of the monomer and does

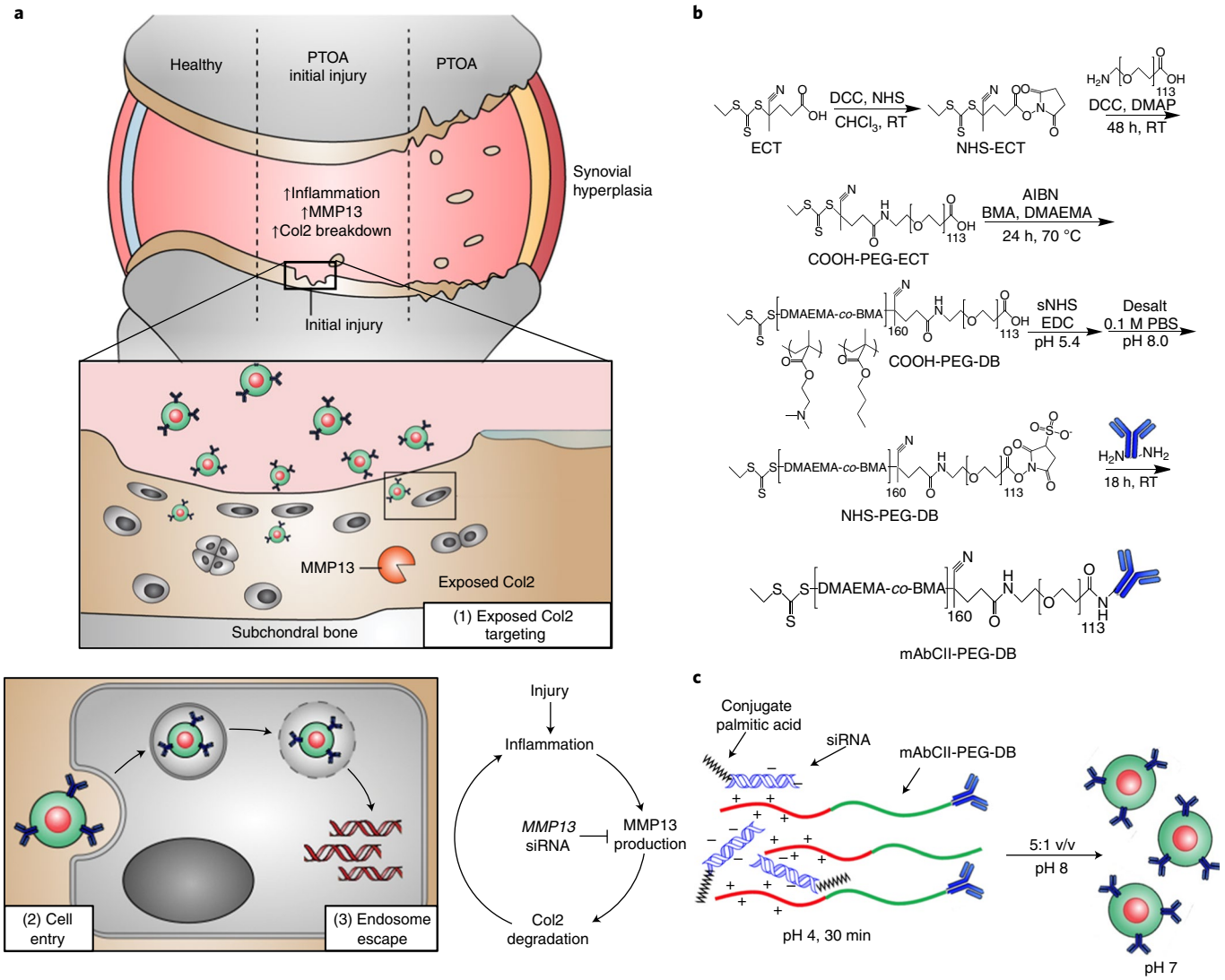


**Fig. 1 | Synthesis of mAbCII-siNPs. a**. Top: schematic illustrating the progression from healthy knee joint (left), to inflammation induction following traumatic injury (middle) and cartilage loss and degenerative joint disease (including synovial response) (right). Degradation of cartilage enhances inflammation, inducing a degenerative cycle (bottom right). Middle, bottom: illustration of the concept of matrix-targeted nanocarriers for enhanced retention and intracellular activity of siRNA at sites of cartilage injury. **b**, Polymer synthesis and mAbCII (blue) conjugation scheme. RT, room temperature; DCC, *N*,*N*′-dicyclohexylcarbodiimide; DMAP, 4-dimethylaminopyridine; AIBN, azobisisobutyronitrile. **c**, Formulation schematic for siRNA cargo loading and assembly of mAbCII-siNPs. First, the polymer is dissolved in a pH 4 solution (to protonate DMAEMA, making it more positively charged). This solution is then mixed with the negatively charged siRNA (with lipid tail to interact better with the BMA component of polymer) for 30 min to allow electrostatic siRNA complexation by the polymer. Next, a 5:1 v/v of pH 8 buffer to complexed siRNA/polymer pH 4 solution is added dropwise to adjust the solution to physiologic pH of 7.4. Red, cationic and endosomolytic DB component of polymer; green, colloidally stabilizing PEG component of polymer; blue, mAbCII monoclonal antibody.

not remove the native epitope; unless the collagen is newly synthesized, non-enzymatic cross-links formed over time maintain the monomer in the fibrillar structure upon trypsin exposure. Trypsin pre-treatment was used in the screening model to mimic damage from OA and because the mAbCII antibody preferentially binds to Col2 that becomes accessible when cartilage is mechanically or proteolytically damaged[44,45]. The mAbCII-siNPs were prepared with molar ratios of non-conjugated polymer:antibody-modified polymer ranging from 20:1 to 80:1. The polymers used comprised rhodamine acrylate (excitation/emission wavelength, 548/570 nm) copolymerized at 1 mol% in the poly(DMAEMA-*co*-BMA) block to enable fluorescent measurement of carrier retention on the damaged cartilage plugs. Retention of siNPs on trypsin-damaged cartilage after washing with phosphate-buffered saline (PBS) was quantified by IVIS imaging and showed that conjugation of mAbCII to the polymer at 40:1 polymer:mAbCII molar ratio provided the best retention performance (Fig. 2f and Supplementary Fig. 4a). These data confirm that mAbCII conjugation enhances binding of siNPs to exposed Col2 in damaged cartilage and motivated our focus on the 40:1 conjugation ratio for subsequent studies. The optimized mAbCII-siNP formulation was also confirmed to preferentially bind to trypsin-damaged cartilage over undamaged cartilage plugs (Fig. 2g).

Subsequently, the porcine cartilage binding assay was adapted to confirm whether matrix-bound mAbCII-siNPs could achieve effective substrate-mediated siRNA delivery and bioactivity. Following incubation of all siNP groups loaded with anti-luciferase siRNA (siLuciferase) with trypsin-damaged cartilage, a PBS washing step

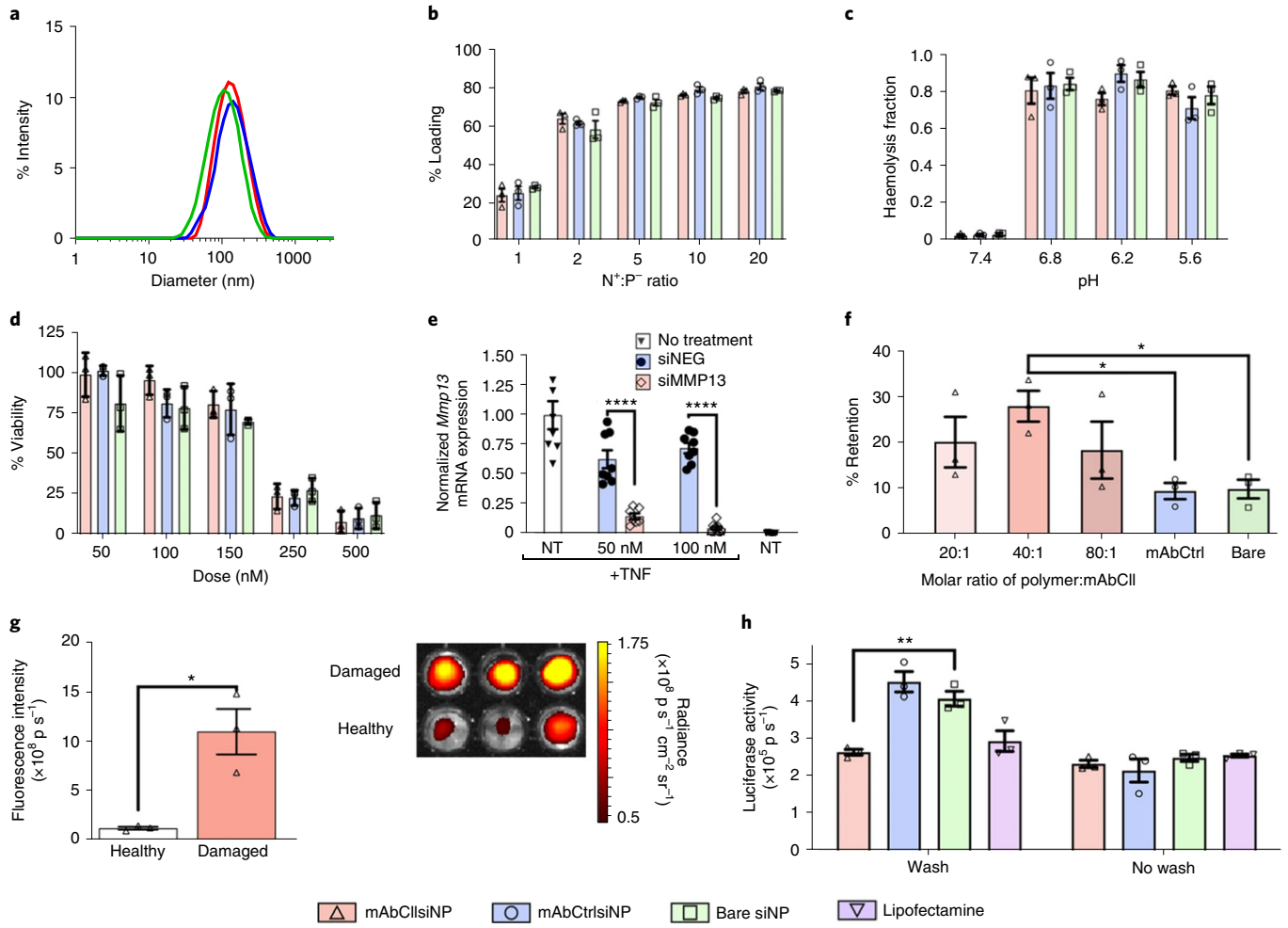


**Fig. 2 | Characterization of in vitro chemico-physical, gene silencing and cartilage retention of mAbCII-siNPs relative to bare and mAbCtrl-functionalized siNPs. a**, siNP sizing by dynamic light scattering. **b**, siRNA encapsulation by Ribogreen assay ($n=3$ technical replicates) where $N^+:P^-$ is the ratio of positive nitrogen groups ($N^+$) in polymer side chains to negative phosphate groups ($P^-$) in the siRNA cargo backbone. Percentage calculation is based on Ribogreen fluorescence of free siRNA at the same concentration. **c**, pH-triggered membrane disruption by haemolysis assay ($n=3$ technical replicates). **d**, Dose-dependent cytocompatibility of siNPs in ATDC5 cells ($n=3$ biological replicates) as measured using a luminescent cell viability assay. Percentage calculation is based on luminescence of untreated cells cultured in parallel in otherwise equivalent conditions. **e**, *Mmp13* silencing by mAbCII-siNPs in ATDC5 cells stimulated with TNF (siMMP13 versus 50 nM or 100 nM siNEG: $P<0.0001$; one-way analysis of variance (ANOVA) followed by Tukey's test for multiple comparisons ($\alpha=0.05$); $n=7$ biological replicates for untreated groups (NT) with or without TNF, $n=9$ biological replicates for treated groups; gene expression normalized to that of untreated, TNF-stimulated cells). **f**, Retention of siNPs (as measured by IVIS imaging of polymer rhodamine fluorescence) with different polymer:mAbCII molar ratios on trypsin-damaged porcine cartilage explants (40:1 mAbCII-siNP versus bare-siNP: $P=0.039$, 40:1 mAbCII-siNP versus mAbCtrl-siNP: $P=0.034$; one-way ANOVA followed by Dunnett's test for multiple comparisons ($\alpha=0.05$); $n=3$ cartilage explant biological replicates; percentage calculation based on the fluorescence of cartilage samples after removal of treatment medium but before washing). **g**, Retention of mAbCII-siNPs on healthy and trypsin-damaged porcine cartilage explants, as measured by intravital IVIS imaging of polymer fluorescence, rhodamine. Area and solid angle remained constant between all measurements (healthy versus damaged: $P=0.0132$; images show 3 technical replicates; unpaired two-sided *t*-test). **h**, Substrate-mediated gene silencing of *Mmp13* in vitro is enhanced by mAbCII-siNP binding and retention on trypsin-damaged porcine cartilage. One-way ANOVA followed by a Tukey's test for multiple comparisons ($\alpha=0.05$); mAbCII-siNP versus bare-siNP: $P=0.008$; $n=3$ cartilage explant biological replicates; area and solid angle remained constant between all measurements; $^*P<0.05$, $^{**}P<0.01$, $^{****}P<0.0001$. Data are mean ± s.e.m.

was done to simulate synovial fluid clearance. Chondrogenic ATDC5 cells that were lentivirally transduced with a constitutive luciferase reporter were then seeded over the damaged cartilage that had been pre-treated with mAbCII-siNPs, bare-siNPs or mAbCtrl-siNPs. In parallel, the same groups were run without the washing step to experimentally dissect the benefit of siNP matrix binding and retention. Significantly higher luciferase silencing was observed with mAbCII-siNPs compared with bare-siNPs and mAbCtrl-siNPs when a wash step was used before cell seeding (Fig. 2h). These data confirm a potential pharmacokinetic benefit of siNP matrix binding and that substrate-mediated delivery of matrix-targeted siNPs achieves target-gene silencing.

**In vivo Col2-anchoring-dependent *Mmp13* silencing.** An acute PTOA model of noninvasive repetitive joint loading was used by subjecting the left knee of 8-week-old C57BL/6 mice to 500 cycles of compressive mechanical loading at 9 N (Fig. 3a). This procedure was repeated three times per week over a period of two weeks using conditions adapted from previous studies[38,46]. Following loading, mice were treated by intra-articular injection of 0.5 mg kg$^{-1}$

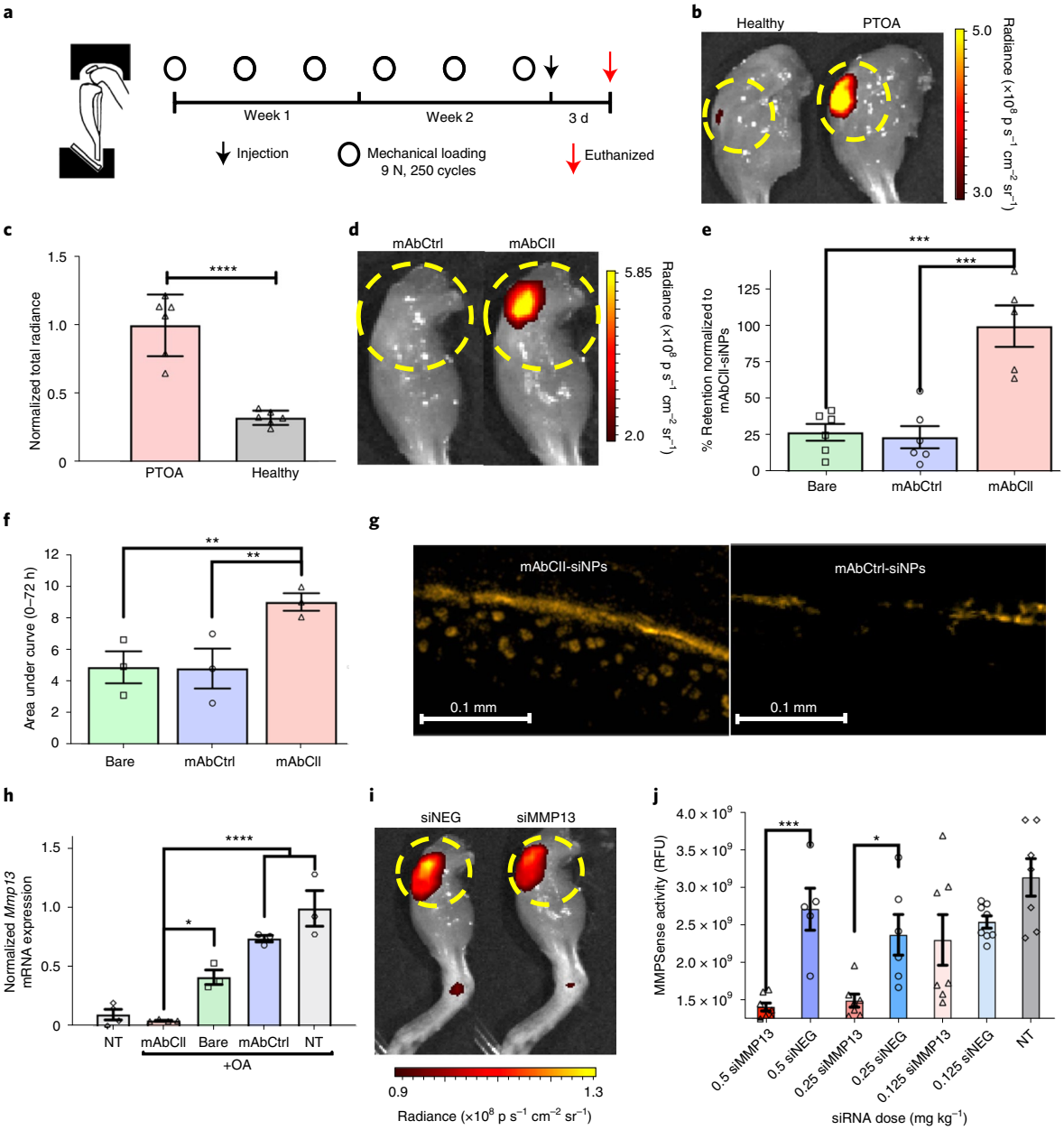


**Fig. 3 | mAbCII-siNP/siMMP13 is retained locally and potently silences *Mmp13* expression relative to bare and mAbCtrl-functionalized siNPs in the knee joints of a short-term mouse model of PTOA. a**, Schematic of the mouse knee mechanical loading apparatus (TA instruments ElectroForce 3100 with a custom 3D-printed fitting for the mouse knee and for the ankle and leg) with the corresponding loading regimen used in the short-term PTOA model studies. **b**,**c**, Intravital imaging (**b**) and quantification (**c**) of mAbCII-siNP retention in healthy versus PTOA knee joints. Yellow dashed circles represent the area in which fluorescence is quantified. Fluorescence is normalized to background signal in PTOA joints with no treatment. PTOA versus healthy: $P < 0.0001$; $n = 6$ knees as biological replicates. **d**,**e**, Representative ex vivo imaging (**d**) and quantification (**e**) of retention of mAbCII-siNPs as compared with mAbCtrl-siNPs and bare-siNPs in PTOA knee joints explanted at 3 days. Yellow dashed circles represent area of quantified fluorescence. mAbCII-siNP versus bare-siNP: $P = 0.0002$, mAbCII-siNP versus mAbCtrl: $P = 0.0001$; mAbCII-siNP: $n = 5$; other groups: $n = 6$ knee joints as biological replicates. **f**, In vivo PTOA knee joint retention of bare-siNPs, mAbCII-siNPs and mAbCtrl-siNPs presented as pharmacokinetic area under the curve calculated from intravital imaging over 3 d after treatment. mAbCII-siNP versus bare-siNP: $P = 0.003$; mAbCII-siNP versus mAbCtrl-siNP: $P = 0.003$; $n = 3$ mice. **g**, Cartilage penetration and retention of mAbCII-siNPs versus mAbCtrl-siNPs 12 h after injection into PTOA knee joints tracked by rhodamine-labelled siNPs (orange). A representative image was selected from three different knee joint samples, on the basis of quality and intactness of tissue cryosection. **h**, In vivo gene expression of *Mmp13* measured by RT–qPCR in mouse knees treated with 0.5 mg kg$^{-1}$ siRNA per knee using mAbCII-siNPs, mAbCtrl-siNPs or bare-siNPs. mAbCII-siNP versus bare-siNP: $P = 0.012$; mAbCII-siNP versus mAbCtrl-siNP and no treatment (NT) with PTOA: $P < 0.0001$; $n = 3$–4 knee joints as biological replicates; RNA expression normalized to untreated, PTOA. **i**,**j**, Representative images of total MMP activity as visualized with MMPSense probe with 0.5 mg kg$^{-1}$ siRNA (**i**) and total MMP activity with varying siRNA doses (**j**). Yellow dashed circles represent area of quantified fluorescence. siMMP13 versus siNEG 0.5 mg kg$^{-1}$: $P = 0.0008$; siMMP13 versus siNEG 0.25 mg kg$^{-1}$: $P = 0.027$; $n = 5$–8 knee joints as biological replicates; $n$ of progressive-dose groups varies due to disqualification at time of injection because of failed injections. $^*P < 0.05$, $^{**}P < 0.01$, $^{***}P < 0.001$. Unpaired two-sided $t$-tests (**c**,**j**); one-way ANOVA followed by Tukey's test for multiple comparisons ($\alpha = 0.05$) (**e**,**f**,**h**); data are mean ± s.e.m. RFU, relative fluorescence units.

per knee of formulated siRNA with mAbCII-siNPs, bare-siNPs or mAbCtrl-siNPs. All forms of siNPs contained a rhodamine acrylate monomer integrated into the poly(DMAEMA-*co*-BMA) block that forms the NP core, enabling pharmacokinetics to be assessed using IVIS fluorescence imaging.

To compare in vivo retention of mAbCII-siNPs between healthy (unloaded) and PTOA (loaded) knees, explanted knees were imaged at 72 h after injection (Fig. 3b), revealing that mAbCII-siNPs were preferentially retained in PTOA over non-injured knees (Fig. 3c). The mAbCII-siNPs also showed significantly better retention within PTOA joints compared with mAbCtrl-siNPs and bare-siNPs (Fig. 3d–g and Supplementary Fig. 4b). We also measured biodistribution to the major clearance organs, including liver, kidney and spleen, using IVIS imaging. The mAbCII-siNP retention in the PTOA knee reduced biodistribution to the liver compared with mice without PTOA that were intra-articularly injected with mAbCII-siNPs (Supplementary Fig. 5a,b). To confirm whether mAbCII-siNPs achieved cartilage penetration and delivery to the chondrocytes, cryosections were imaged from knees explanted 12 h after intra-articular injection (Fig. 2g). mAbCII-siNPs were observed at the articular cartilage surface and also concentrated in individual chondrocytes (orange signal); there was also some mAbCtrl-siNPs signal at the articular cartilage surface, but there was no evidence of retention within the chondrocyte niche. The observation of localization both to the articular surface and to the chondrocyte niche are consistent with that previously seen for Col2-targeting peptide-functionalized nanoparticles[27].

Gene silencing activity in vivo in PTOA-affected joints was next compared for mAbCII-siNPs and control formulations injected using the same two-week mechanical loading protocol. Gene-expression analysis on joints collected 3 d after intra-articular treatment confirmed that the ECM anchoring of the mAbCII-siNPs enabled more potent silencing of *Mmp13* expression relative to bare-siNPs or mAbCtrl-siNPs. Treatment with mAbCII-siNPs resulted in more than 90% target-gene knockdown in the mechanically loaded PTOA joints (Fig. 2h). Dose-dependent in vivo gene-silencing activity of mAbCII-siNPs was also measured for 0.125, 0.25 and 0.5 mg kg$^{-1}$ siMMP13 relative to 0.5 mg kg$^{-1}$ siNEG in PTOA knees. At 72 h after treatment, total MMP activity was quantified by IVIS imaging 24 h after intravenous injection with MMPSense (a probe activated by MMP2, 3, 7, 9, 12 and 13). This indicated that the 0.25 and 0.5 mg kg$^{-1}$ siMMP13 doses delivered with mAbCII-siNPs significantly reduced total MMP activity (Fig. 2i,j). In the same experiment, we quantified expression of *Mmp13* and *Il1b* mRNA by RT–qPCR from joint samples collected at 72 h after treatment (Supplementary Fig. 6a,b), motivating our use of a 0.5 mg kg$^{-1}$ per knee dose for subsequent, longer-term studies designed to assess the therapeutic efficacy of mAbCII-siNPs and mAbCII-siMMP13 treatments as DMOADs. We also assayed the longevity silencing at the 0.5 mg kg$^{-1}$ dose (Supplementary Fig. 6c), motivating the use of a weekly dose in subsequent studies.

***Mmp13* silencing in a longer-term OA mouse model.** A six-week study was completed to evaluate the therapeutic effect of weekly doses of *Mmp13*-silencing mAbCII-siNPs in a mouse model of longer-term and more aggressive PTOA. Tests for this model were carried out in C56BL/6 mice aged up to 6 months and subjected to a more rigorous cyclic mechanical loading protocol[47] of 9 N, 500 cycles, 5 times per week for 6 weeks (Fig. 4a). Doses of 0.5 mg kg$^{-1}$ siRNA were administered to each knee weekly, starting concurrently with mechanical loading. MMPSense and Alexa Fluor-labelled mAbCII antibody were injected intravenously 24 h before mice were killed to gauge total MMP activity and quantify cartilage damage, respectively. Even though the mice were analysed a full week following administration of the final dose, the reduction in *Mmp13* expression achieved with mAbCII-siNPs was consistent with the short-term model, with a decrease of more than 80% compared with OA joints treated with siNEG using mAbCII-siNPs (Fig. 4b). Immunohistochemical staining revealed that MMP13 production in both the articular cartilage and the synovial tissue was reduced by treatment with siMMP13 delivered by mAbCII-siNPs (mAbCII-siNP/siMMP13) (Fig. 4c,d). The inflammation associated with PTOA is characterized by detrimental tissue restructuring potentiated by cytokines and growth factors produced in the synovium of the joint[48]. Degradation products of Col2 have signalling properties that contribute to catabolic activity, hypertrophy and apoptosis[49]. The mAbCII-based retention of siMMP13 in the PTOA joint provide primary, cartilage-protective effects as well as secondary effects associated with reduced production of degradation products that initiate downstream production of inflammatory cytokines and MMPs by the synovium.

Histological analysis showed that mAbCII-siNP/siMMP13 treatment significantly reduced PTOA-associated joint-structural changes. Coronal sections of fixed knee joints were stained with safranin O and fast green to evaluate cartilage histopathology (Fig. 4e and Supplementary Fig. 7). Sections were then blindly scored by a trained pathologist using the criteria outlined in Supplementary Table 2a,b. Safranin O stains proteoglycans associated with normal cartilage a deep red and is used for histopathological scoring of cartilage as recommended by the Osteoarthritis Research Society International (OARSI)[50]. The reduced safranin O staining and surface discontinuity observed in untreated OA and siNEG-treated OA is indicative of proteoglycan loss and cartilage erosion and was markedly improved in siMMP13-treated joints, as reflected in the disparate OARSI scores between treatment groups (Fig. 4f).

Total MMP activity was also significantly reduced in the mAbCII-siNP treated mice compared with controls that were either untreated or treated with mAbCII-siNPs loaded with siNEG (Fig. 4g). Relative binding of Alexa Fluor-labelled mAbCII antibody to pathologically exposed Col2 is a biomarker for degree of cartilage damage[38,51,52] and was thus used here as an intravital readout for disease severity. Significantly greater binding of mAbCII was observed in untreated mice and mice treated with mAbCII-siNP/siNEG compared with mice treated with mAbCII-siNP/siMMP13, indicating that *Mmp13* silencing protected the cartilage structure (Fig. 4h,i). Levels of Alexa Fluor 680–mAbCII binding in the PTOA joint were similar between untreated mice and mAb-Col2-siNP/siNEG-treated mice, indicating that treatment with mAbCII-functionalized siNPs one week earlier did not in itself interfere with the subsequent mAbCII-based cartilage damage measurement.

Haematoxylin and eosin (H&E) staining was used to evaluate overall joint status, including response in the meniscus and synovium (Fig. 5a and Supplementary Fig. 8). Joint mechanical loading induced robust synovial thickening, osteophytes and mineralization in the meniscus. Whole-joint histology was blindly scored by a pathologist (Fig. 5b) based on the degenerative joint disease (DJD) criteria outlined in Supplementary Table 2. While cartilage structure was strongly protected by mAbCII-siNP/siMMP13 treatment (treated mice did not have statistically different OARSI score compared with normal mice with no load-induced PTOA), it also better preserved the normal structure of the synovium and meniscus compared with control-treated mice. H&E staining of joint sections for siNEG and untreated groups consistently showed more synovial hyperplasia, larger osteophytes and more mineralization in the menisci compared with the mAbCII-siNP/siMMP13 group. Use of micro-computed tomography (microCT) to more globally visualize and quantify ectopic mineralization revealed that mAbCII-siNP/siMMP13 treatment significantly protected against meniscal mineralization and osteophyte formation (Fig. 5c–g and Supplementary Fig. 9a). These data support that *Mmp13* silencing provides secondary benefits to the joint in addition to directly reducing articular cartilage loss.

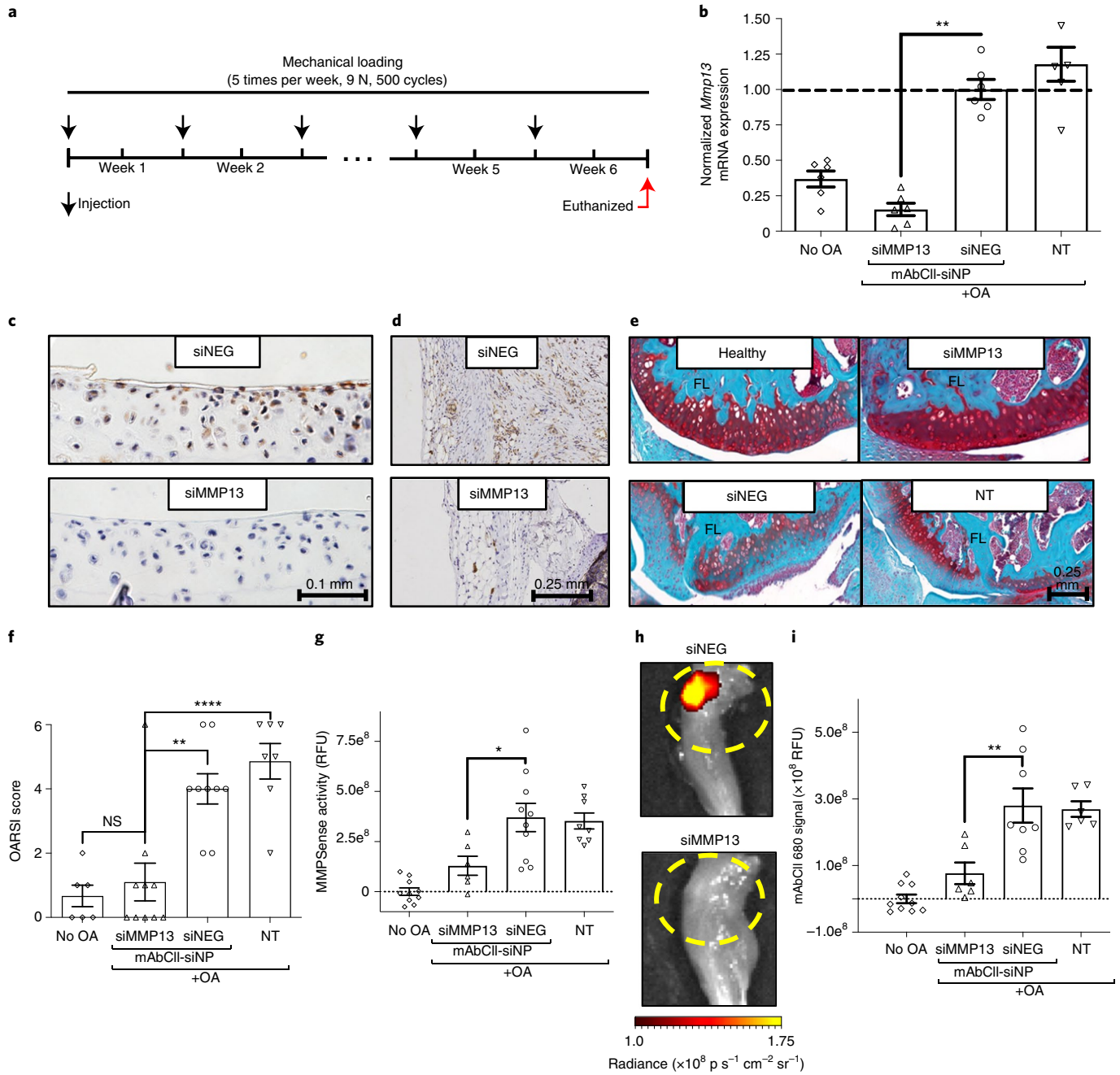


**Fig. 4 | Long-term *Mmp13* silencing reduces MMP13 protein levels in cartilage and synovium and protects mechanically loaded joints from OA progression. a**, Loading and treatment regimen used in the long-term PTOA mouse model. **b**, *Mmp13* expression at the end of week 6 (siMMP13 versus siNEG: $P < 0.0001$; $n = 5$–6 knee joints as biological replicates; RNA expression normalized to the average of the siNEG-treated PTOA joints. **c**, Immunohistochemical staining of MMP13$^+$ regions (brown) of the tibial articular cartilage treated with siNEG (top) and showing reduced MMP13 protein levels when treated with mAbCII-siNPs/siMMP13 (bottom). **d**, Immunohistochemical staining of MMP13$^+$ regions (brown) of the synovial tissue treated with siNEG (top) and showing reduced MMP13 protein levels when treated with mAbCII-siNPs/siMMP13 (bottom). Images in **c**,**d** are representative of three independent samples based on the most intact tissue section for each group. **e**, Representative safranin O staining of the articular surface of the femur in healthy mice (top left) and PTOA mice treated with siMMP13 (top right), siNEG (bottom left) or no treatment (bottom right); FL, lateral femoral condyle. **f**, Quantification of cartilage damage using the OARSI OA cartilage histopathology assessment system (**e**,**f**; siMMP13 versus no OA: $P = 0.99$, siMMP13 versus siNEG: $P = 0.001$, siMMP13 versus no treatment: $P < 0.0001$; $n = 6$–9 knee joints as biological replicates with each replicate imaged. **g**, Total MMP activity at 6 weeks measured by MMPSense probe, normalized to mean MMPSense fluorescence in healthy knees without PTOA; siMMP13 versus siNEG: $P = 0.016$; $n = 6$–10 knee joints as biological replicates. **h**,**i**, Representative images (**h**) and quantification (**i**) of the binding of fluorescently labelled mAbCII in the knee joint at six weeks as a marker for relative cartilage damage and resultant exposure of Col2. siMMP13 versus siNEG: $P = 0.002$; $n = 6$–10 knee joints as biological replicates, with each replicate imaged separately. $^*P < 0.05$, $^{**}P < 0.01$, $^{***}P < 0.001$, $^{****}P < 0.0001$. *n* of groups varies due to disqualification at time of injection because of failed intra-articular injections of treatments, failed tail-vein injection of mAbCII 680, or failure to retrieve adequate sections for histological scoring. One-way ANOVA followed by Tukey's test for multiple comparisons ($\alpha = 0.05$) (**b**,**f**,**g**,**i**). Data are mean ± s.e.m. RFU, relative fluorescence units.

When evaluating OA joints clinically, the presence of osteophytes and ossified nodules within the meniscus and synovium is especially important, as these characteristics are used to gauge OA progression and appear in the most advanced stages of the disease[50,53]. These rigid calcium deposits are associated with synovial macrophage activation in experimental OA[54], where they concentrate local mechanical stress. Further, presence of calcium phosphate can exacerbate synovitis by activating inflammasomes and consequently triggering production of the OA driver IL-1β[55]. While inflammation affects patient comfort, complications and acute pain from osteophytes and calcium deposits are often cited as primary reasons for patients with advanced OA to resort to total knee replacement[56]. Inhibiting pathological ossification would be anticipated to enable maintenance of an active lifestyle and to delay total knee replacement.

To investigate the joint and surrounding tissues more broadly, we characterized subchondral trabecular bone using microCT. Of note, mAbCII-siNP/siMMP13 treatment significantly reduced loss of subchondral trabecular bone volume associated with PTOA (Supplementary Fig. 9b). Tartrate-resistant acid phosphatase staining was also performed to assess osteoclast activity as a snapshot of bone resorption (Supplementary Fig. 9c). There was an increase in activated osteoclasts in untreated, mechanically loaded knees compared with those receiving mAbCII-siNP/siMMP13 treatment. These data reinforce the complexity of OA as a full-joint disease, while also indicating that *Mmp13* RNAi has beneficial, global impacts within the joint by also affecting cartilage crosstalk with surrounding tissue. There is strong clinical precedent for observing multiple, concomitant types of aberrant mineral homeostasis within the OA joint. Clinically, calcium deposits often manifest in the meniscal and synovial tissue and fluid. At the same time, pathological vascularization and thickening of the subchondral bone plate can cause loss of subchondral trabecular bone[55]. Animal models and human samples suggest an influence of MMP13 and cathepsin K, specifically, in driving pathological subchondral bone resorption in late-stage OA in human tissues[57]. In accordance with these studies, we find that subchondral bone resorption and pathologic bone restructuring within the whole joint are reduced with MMP13 inhibition.

The rigorous model used in this study induced several aspects of joint pathology observed clinically, including articular cartilage loss, soft tissue mineralization, osteophyte formation and remodelling of subchondral bone. This model is based on repeated mechanical loading of the joint in flexion rather than a single surgical or injury procedure that induces a torn or transected ligament, as is commonly used to model PTOA. The model using repeat mechanical loading has been validated in previous publications[46]. One benefit of this model is that it does not require an invasive surgical procedure that can itself damage the joint. Moreover, we observe a more consistent phenotype and less variation than with surgical models because the joint injury is created by the cumulative effect of multiple loading sessions over time using a highly controlled mechanical testing apparatus. Importantly, the repeated mechanical loading model reproduces many of the characteristics of other preclinical models of PTOA and of clinical PTOA, including cartilage deterioration, heterotopic ossification and inflammation[58]. The model that we use here is also comparable to a related load-induced PTOA model that uses mechanical loading to tear the anterior cruciate ligament[59]. The overload-induced anterior cruciate ligament tear model is characterized by considerable joint-structural changes, with osteophytes forming on the anteromedial aspect of the distal femur and the posteromedial aspect of the proximal tibia, in addition to ectopic mineralization occurring in the medial meniscus[59], analogous to the joint effects seen in our studies (Figs. 4 and 5). It will be of interest to test our experimental therapy in larger animal models in which joint dimensions and OA pathogenesis more closely resemble those in humans.

***Mmp13* silencing broadly affects OA-associated gene expression.** Targeting *Mmp13* directly using RNAi was found to have broad effects on overall joint health, including on both the articular cartilage and surrounding hard and soft tissues. To further characterize the global effects of targeted MMP13 inhibition, the mechanical loading mouse model was repeated with the same parameters except that samples were collected at 4 weeks rather than 6 weeks to capture a more intermediate stage of disease (Fig. 6a). The nanoString nCounter Inflammation panel was used to quantify expression of 254 genes in the knee joint samples (articular cartilage, meniscal and synovial tissue). Unsupervised analysis using nanoString software indicated that the joints treated with mAbCII-siNPs/siMMP13 were more similar to normal tissue and more different from untreated OA tissue than those treated with mAbCII-siNPs/siNEG (Fig. 6b). Compared with treatment with mAbCII-siNPs/siNEG, treatment with mAbCII-siNPs/siMMP13 significantly suppressed expression levels of several clusters of genes with notable associations with OA progression (Fig. 6c,d).

In PTOA joints, mAbCII-siNPs/siMMP13 treatment significantly reduced clusters of genes associated with tissue restructuring and angiogenesis. Tissue remodelling is an active process in response to injury in the articular cartilage and especially in the synovium, where capsule thickening, vascularization and hyperplasia occur. These processes are associated with the upregulation of genes such those encoding MEF2α (associated with chondrocyte hypertrophy) and PDGFα (a potent synovial fibroblast growth factor)[60,61], which were suppressed by mAbCII-siNPs/siMMP13. *Mmp13* silencing also suppressed the VEGF receptor Flt-1, which is predominantly expressed by vascular endothelial cells and is involved in angiogenesis. The less active tissue remodelling and thickening processes in

**Fig. 5 | mAbCII-siNP/siMMP13 treatment provides whole-knee-joint protection by reducing synovial thickening, osteophyte formation and meniscal mineralization. a**,**b**, H&E staining of knee joints, focusing on the synovial and meniscal regions (**a**) and average DJD score by treatment group (**b**). Histological scoring (using the criteria in Supplementary Table 2) was completed by a treatment-blinded histopathologist (siMMP13 versus siNEG: $P=0.042$; $n=4$–6 knee joints ($n=4$ for healthy and untreated PTOA mice, $n=5$ for siNEG, $n=6$ for siMMP13) as biological replicates). **c**, MicroCT 3D renderings of meniscal–ectopic mineralization and osteophyte growth in healthy control and PTOA mice treated with siMMP13, siNEG or with no treatment. Arrows indicate meniscal–ectopic mineralization; pound signs indicate osteophytes. **d**, MicroCT 3D rendering of osteophytes (marked with red arrows) in knee joints from a healthy control mouse (top left) and in PTOA mice treated with siMMP13, siNEG or with no treatment. **e**, Cross-sectional microCT views used to measure osteophyte outgrowth size (red bar) in knee from a healthy control mouse (top left) and in PTOA mice treated with siMMP13, siNEG or with no treatment. **f**, Quantification of ectopic mineralization (measured by hydroxyapatite (HA) content) in the meniscal and synovial tissues and in the form of osteophytes (siMMP13 versus no OA: $P=0.999$, siMMP13 versus siNEG: $P=0.025$, siNEG versus no treatment: $P=0.88$; $n=5$–6 knee joints ($n=5$ for siMMP13, $n=6$ for all other groups) as biological replicates). **g**, Measurements of both tibial and femoral osteophyte size at the site of the largest outgrowth from normal cortical bone structure. Tibial: siMMP13 versus no OA: $P=0.999$, siMMP13 versus siNEG: $P=0.005$, siNEG versus no treatment: $P=0.25$; femoral: siMMP13 versus no OA: $P=0.72$, siMMP13 versus siNEG: $P<0.0001$, siNEG versus no treatment: $P=0.64$; $n=6$ knee joints as biological replicates. Data are mean ± s.e.m. $^{*}P<0.05$, $^{**}P<0.01$, $^{***}P<0.001$, $^{****}P<0.0001$, NS, not significant. One-way ANOVA followed by Tukey's test for multiple comparisons ($\alpha=0.05$) (**b**,**f**,**g**).

joints treated with mAbCII-siNP/siMMP13 were also associated with suppression of gene clusters related to proteolysis and skeletal development. *Mmp13* silencing also led to downregulation of genes associated with apoptosis, such as *Jun* (which also induces *Mmp13* expression) and the inflammatory cytokine IL-6, which is mechanistically involved in propagation of cellular stress and synovial inflammation[62,63].

Treatment-associated downregulation of genes related to tissue restructuring, apoptosis, angiogenesis and proteolysis were also complemented by reduction of innate immune activation in joints with targeted *Mmp13* silencing. Expression of prostaglandin-endoperoxide synthase 2 (PTGS2), an inflammation driver that encodes cyclooxygenase 2 (COX2), was significantly reduced in mechanically loaded joints with mAbCII-siNP delivery of

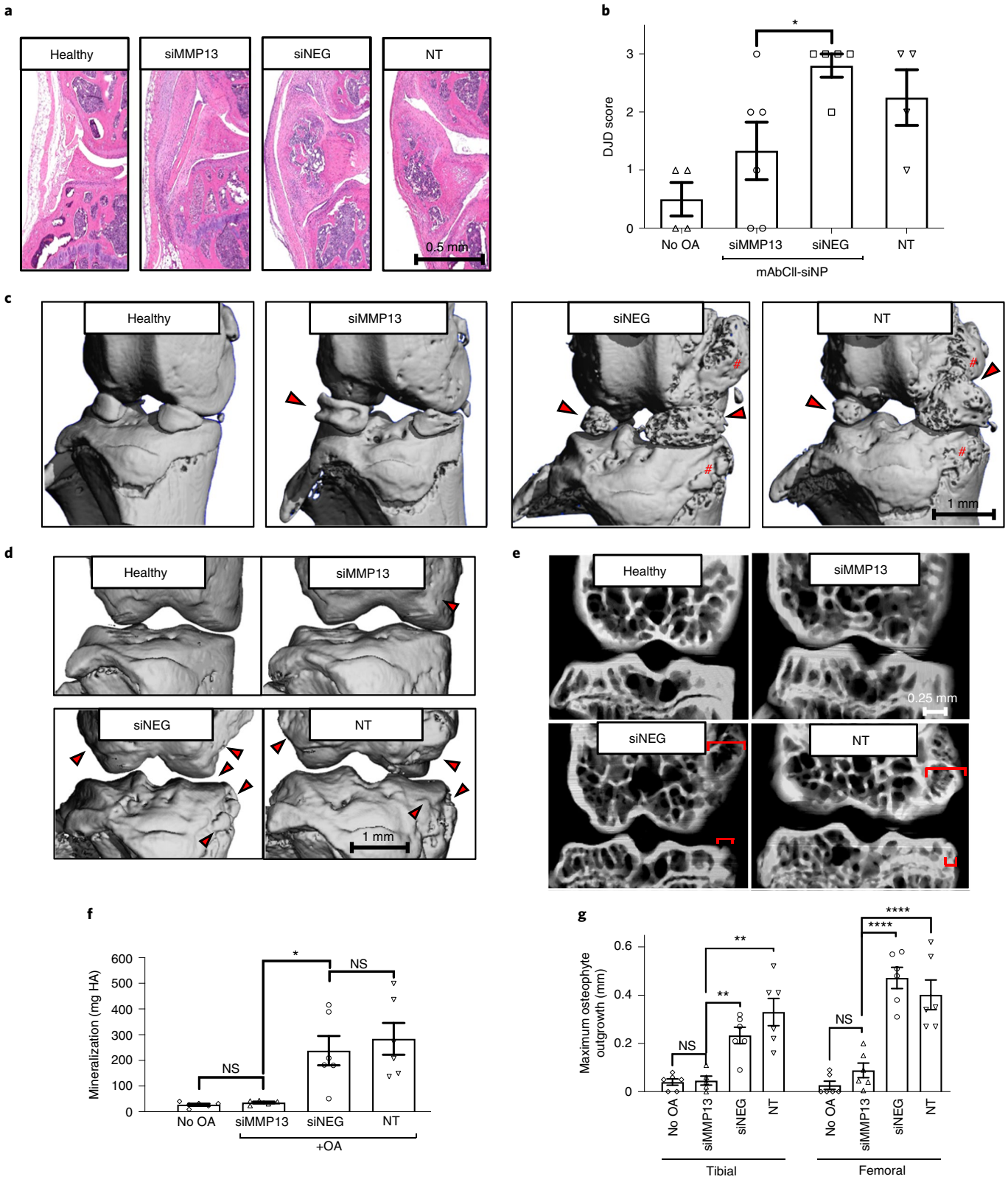

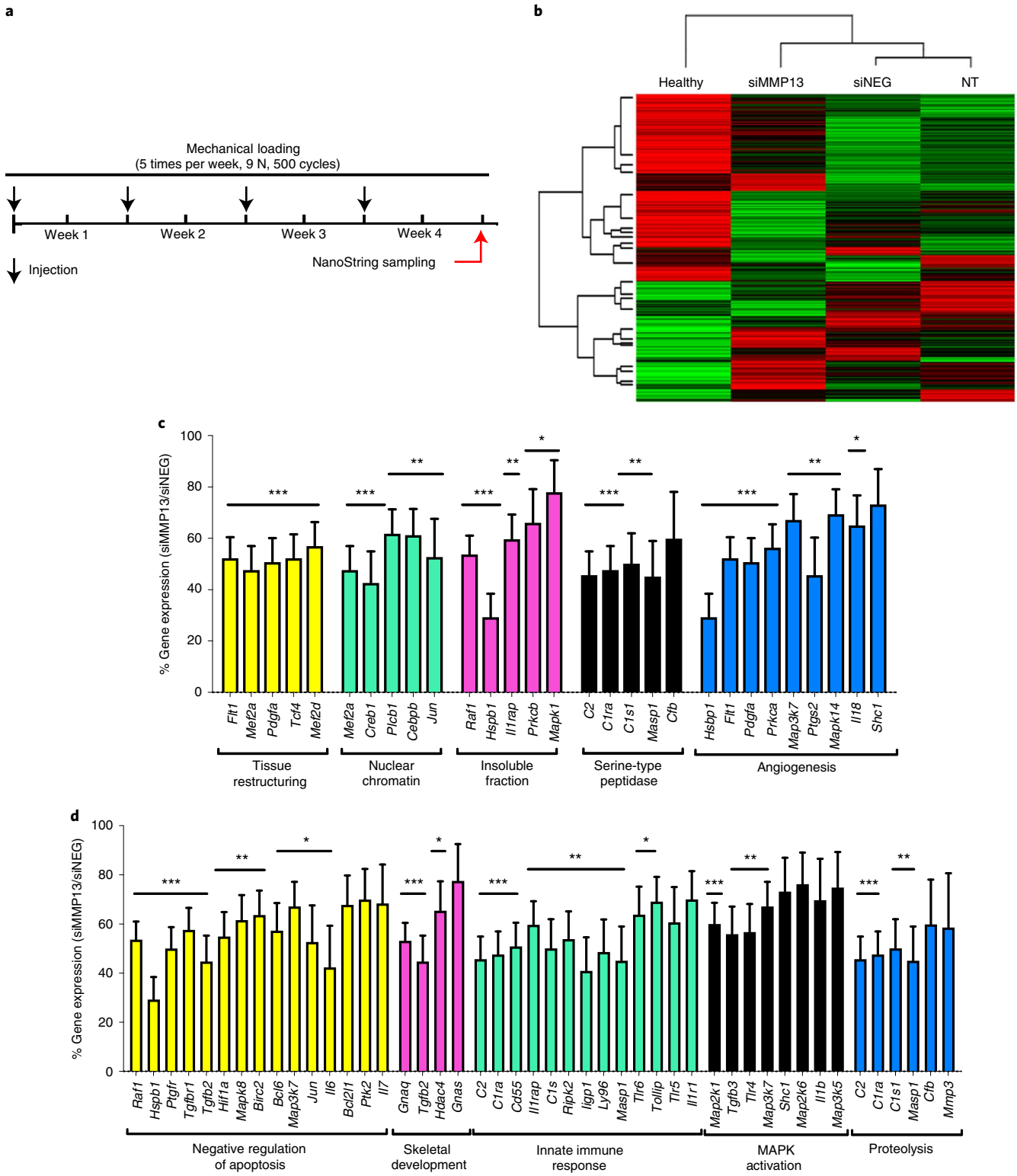


**Fig. 6 | Mmp13 silencing by mAbCII-siNP/siMMP13 treatment globally impacts gene-expression patterns in mechanically loaded PTOA joints.** **a**, Loading and treatment regimen used for the nanoString analysis study. **b**, Unsupervised sorting of treatment groups from highest to lowest similarity in gene expression patterns relative to healthy (non-PTOA) joints at the end of a 4-week study. Gene expression is shown as high (green) or low (red) expression, sorted vertically by differences between treatment groups. **c**,**d**, Gene clusters were significantly different between siNEG- and siMMP13-treated joints. Five most changed gene clusters (**c**) and next five most changed (**d**). Gene expression is normalized to six internal reference genes (*Cltc*, *Gapdh*, *Gusb*, *Hprt*, *Pgk1* and *Tubb5*). The plots are arranged such that the clusters' *P* values between siMMP13 and siNEG treatment groups are lowest on the left and highest on the right. $n = 4$–8 knee joints (biological replicates: $n = 4$ for healthy, $n = 6$ untreated and $n = 8$ for siMMP13 and siNEG) with triplicate technical measurements; statistical analysis of all groups was conducted using nanoString software to perform one-way ANOVA followed by Tukey's test for multiple comparisons ($\alpha = 0.05$); $^{*}P < 0.05$, $^{**}P < 0.01$, $^{***}P < 0.001$. Data are mean ± s.e.m. The complete nanoString dataset is available in the Gene Expression Omnibus under accession GSE171031.

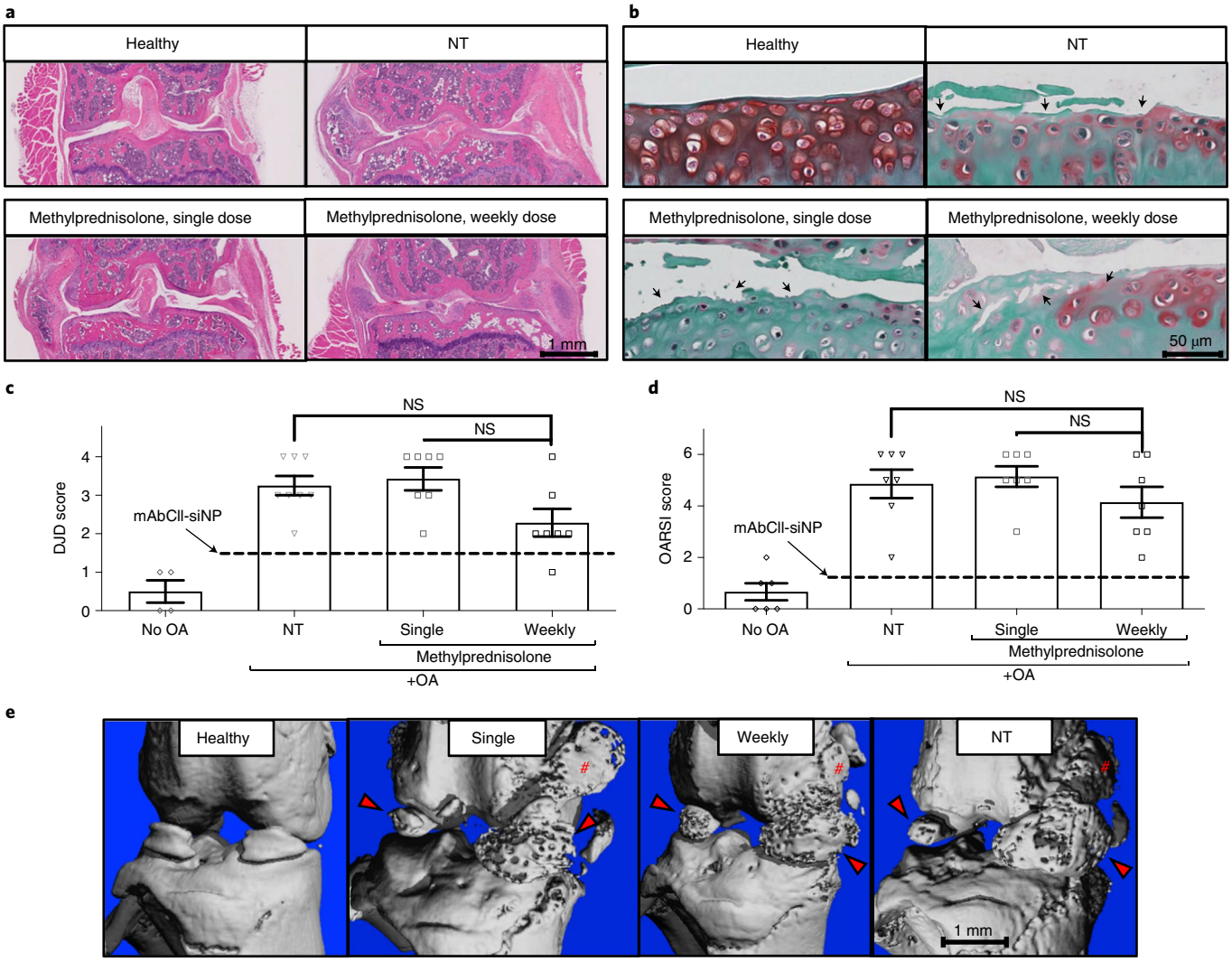


**Fig. 7 | Clinical gold standard steroid treatment with methylprednisolone does not provide DMOAD effects in a long-term PTOA mouse model, unlike mAbCII-siNP/siMMP13 treatment. a**, Representative whole-joint histological sections stained with H&E after six weeks in a healthy control (top left), and in PTOA mice with no treatment, a single dose of methylprednisolone or a weekly dose of methylprednisolone. **b**, Representative safranin O staining of the articular surface of the tibia and femur after six weeks in a healthy control (top left), and in PTOA mice with no treatment, a single dose of methylprednisolone or a weekly dose of methylprednisolone. Arrows highlight focal cartilage damage and regions of cartilage degeneration. **c**, Total joint DJD scores were determined from H&E-stained slides by a treatment-blinded histopathologist; mAbCII-siNP/siMMP13 treatment scores were overlaid for comparison (dashed line) (weekly prednisolone versus no treatment: $P=0.73$, weekly prednisolone versus single-dose prednisolone: $P=0.48$; $n=4$–8 knee joints ($n=4$ for healthy mice, $n=8$ for untreated PTOA mice, $n=7$ for one-time and weekly methylprednisolone groups) as biological replicates). **d**, Cartilage integrity was scored using the OARSI OA cartilage histopathology assessment system by a treatment-blinded histopathologist; mAbCII-siNP/siMMP13 treatment scores were overlaid for comparison (dashed line) (weekly prednisolone versus no treatment: $P=0.11$, weekly prednisolone versus single-dose prednisolone: $P=0.057$; $n=6$–7 knee joints ($n=6$ for healthy mice, $n=7$ for all other groups) as biological replicates). **e**, MicroCT 3D reconstructions of osteophytes and ectopic mineralization in meniscus and surrounding tissues after six weeks in a healthy control, and in PTOA mice with a single dose of methylprednisolone, a weekly dose of methylprednisolone or no treatment (left to right) (arrows indicate meniscal mineralization; pound signs indicate osteophyte formations). $n=3$ knee joints as biological replicates rendered by microCT; images for **a**,**b**,**e** were taken for each biological replicate; one-way ANOVA followed by Tukey's test for multiple comparisons ($\alpha=0.05$) (**c**,**d**). Data are mean ± s.e.m.

siMMP13 versus siNEG. This treatment also suppressed expression of *Il1rn*, which encodes the IL-1 receptor antagonist protein (IL1RaP); knockout of this gene correlates with spontaneous arthritis development[64]. Coupled with reduction of innate immune response, *Mmp13* silencing also reduced expression of several serine proteases (C1S, C1RA and C2) that are components of the complement pathway, which is known to be associated with OA progression[65,66]. This suggests that there is less local influx or activation of circulating monocytes, macrophages and monocyte-derived dendritic cells that express C1s, C1RA and C2[67]. *Mmp13* silencing also reduced expression of IL-1β (in the MAPK activation cluster), an inflammatory cytokine that drives OA by inducing nitric oxide production, increasing synthesis of MMPs and aggrecanases, and suppressing proteoglycan synthesis[68]. Interestingly, recent work has highlighted that macrophages present in synovial tissue can induce a pro-inflammatory state[69] and that these cells, in combination with synovial fibroblasts, are primary contributors to MMP13 expression within the joint. MMP13 inhibition directly reduces cartilage degradation, but these larger-scale changes in tissue gene expression further support that this treatment impacts overall joint health; these

broader joint effects may be at least partially due to disrupting the degenerative cycle that is perpetuated by degradative products of the cartilage matrix[16].

The global changes to inflammatory gene expression observed in the present study, in combination with joint analysis utilizing microCT and histology, all support the therapeutic value and safety of local *Mmp13* RNAi nanomedicine that anchors to the cartilage ECM. MMP13 activity within the synovial joint is thought to drive OA progression[70]. By contrast, MMP13 expression by osteocytes is important for normal perilacunar/canalicular remodelling. Selective genetic ablation of MMP13 expression in osteocytes disrupts subchondral bone homeostasis in a way that exacerbates subchondral bone sclerosis and OA pathology[71]. However, the OA phenotype in this mouse model was also associated with a compensatory upregulation of MMP13 expression by the chondrocytes. In light of this observation, the significance of MMP13 inhibition in osteocytes on OA remains an open question. We speculate that a Col2-targeted delivery system such as mAbCII-siNPs, that is injected directly into the intra-articular space, will localize effects to cartilage and adjacent synovial tissues, while any unbound treatment would clear primarily through lymphatic drainage[72], limiting exposure and gene targeting effects on cells embedded within the more remote bone. MicroCT analyses showed that mAbCII-siNP/siMMP13 treatment maintained a more normal subchondral bone volume fraction and reduced both osteophytes and ectopic mineralization, suggesting that matrix-tethering siNPs actually normalized mineralization homeostasis within the joint. This matrix-anchoring system may enable a desirable combination of safe and effective therapeutic MMP13 targeting that may be difficult to achieve with systemic delivery or through delivery of small molecule inhibitors that more readily diffuse into surrounding tissues.

**Benchmark comparisons to clinical standard steroid treatment.** After broadly characterizing the joint-structural and gene-expression implications of mAbCII-siNPs/siMMP13 treatment, the treatment was benchmarked against a current standard therapy using the six-week study protocol. The most prevalent clinical intervention beyond the use of oral nonsteroidal anti-inflammatory drugs is the intra-articular administration of steroids, which are recommended to be given up to four times per year[73]. The most commonly used corticosteroid is methylprednisolone[74]. Because the longer-term, six-week OA mouse model used in our therapeutic studies is aggressive, testing was done for both a single dose of methylprednisolone at the time of first injury (most similar to the frequency of dosing used clinically) and a weekly dose, which was used to match the protocol used for testing of mAbCII-siNPs/siMMP13.

Histological sections of the joints from the steroid-treatment study were blindly scored by a pathologist following H&E and safranin O staining (Fig. 7a–d). Single or weekly methylprednisolone injections did not significantly alter OARSI or DJD scores relative to untreated PTOA knees. These findings are in agreement with other studies demonstrating that while steroids temporarily alleviate inflammatory pain, they have not been demonstrated to protect cartilage structural integrity[12]. Notably, mAbCII-siNPs/siMMP13 treatment significantly reduced both the DJD and the OARSI score relative to controls, whereas single or weekly steroid treatment did not provide any significant protection according to these joint-scoring metrics. Like the histological scoring outcomes, neither steroid-treatment protocol blocked osteophyte formation or ectopic mineralization, unlike mAbCII-siNP/siMMP13 therapy (Fig. 7e). These distinctions further highlight the therapeutic potential of specific inhibition of MMP13, a molecular driver that broadly underlies several aspects of PTOA joint destruction.

## Outlook

RNAi silencing of *Mmp13* using matrix-anchoring nanocarriers to prolong retention within the osteoarthritic joint provides considerable therapeutic benefit in blocking PTOA progression. This study validates the concept that matrix binding for local retention of an in situ-formed nanoparticle-based depot is a viable strategy to improve potency and longevity of action of intracellular biologics such as siRNAs. While formulation of larger (micro-scale) particles may also facilitate retention, it would not be anticipated to be effective for drugs that act intracellularly because of limitations of endocytosis, endosome escape and tissue penetration of larger particles[75]. The treatment described in this study, which uses antibody targeting to reduce joint clearance, achieved target-gene silencing in vivo of up to 90%, with gene silencing remaining potent even 1 week after the final treatment in a 6-week study. Furthermore, local retention of the injected dose and specific targeting of MMP13 are anticipated to reduce the toxicity concerns that have become associated with systemically delivered, non-selective synthetic small molecule MMP inhibitors. The therapeutic relevance of this approach is exemplified in an aggressive, long-term PTOA model, in which treatment resulted in an 80% reduction in *Mmp13* expression, protection of cartilage integrity, improvement in total joint histopathology, reduced ectopic mineralization and osteophyte formation, and less destruction of subchondral bone. None of these beneficial effects were seen with corticosteroid treatment, the clinical standard treatment for OA.

## Methods

**mAbCII antibody.** Monoclonal antibody (E4-D4 clone) raised against bovine Col2 was prepared from a hybridoma clone isolated as previously described[76]. CNBr-derived peptides were obtained by CNBr cleavage of denatured bovine Col2, and the unpurified peptides were separated by PAGE and immunoblotted against the E4-D4 clone.

The clones were characterized by ELISA against native Col2 prepared from mouse, pig, bovine and human cartilage and by western blot analyses against intact and CNBr-derived peptides of bovine Col2 (Supplementary Fig. 1a–c).

**Synthesis and conjugation of polymers.** The synthesis scheme (Fig. 1) was followed as described in the main text, using RAFT polymerization with incremental steps verified by NMR. *N*-hydroxysuccinimide (NHS)-functionalized ECT synthesis was verified by NMR (Supplementary Fig. 2a), and the product was then conjugated to an amine-carboxy heterobifunctional 5 kD PEG to form carboxy-PEG-conjugated ECT for use as an initial chain transfer agent for RAFT polymerization[33]. A co-polymer of DMAEMA and BMA was chain extended from the COOH-PEG-ECT with a desired target degree of polymerization of 150 (1:1 molar ratio of DMAEMA:BMA) to create PEG-DB which was verified by NMR (Supplementary Fig. 2b). The reaction was purged with nitrogen for 30 min. AIBN was used as an initiator (10:1 CTA:initiator ratio) in 10% w/v dioxane. The reaction was stirred at 65 °C for 24 h before precipitation into ether and vacuum drying for 24 h. Polymer was then dissolved and dialysed in methanol for 48 h before transition to dialysis in water for another 48 h.

Subsequently, a two-stage sulfo-NHS–EDC conjugation protocol was optimized for activating the polymer and removing excess activating compounds before mixing of the polymer with the antibody to avoid antibody crosslinking. Carboxyl-terminated PEG-DB polymer was dissolved in ethanol at a 20 mg ml$^{-1}$ concentration before addition to 0.05 M MES buffer, pH 6.0 to prepare a final 1 mg ml$^{-1}$ solution of COOH-PEG-DB polymer. EDC and sNHS were added at 250 and 500 mM, respectively, and allowed to react for 15 min at room temperature. Excess EDC and sNHS were then eliminated using 10 kD MWCO spin filters from Amicon, centrifuging at 3,000 rcf for 13 min from an initial volume of 6 ml. The total volume was then reconstituted to 6 ml by addition of more MES buffer. Antibody at 1 mg ml$^{-1}$ in 0.1 M PBS, pH 8.0 was added to the activated polymer solution and allowed to react for 18 h at room temperature. Conjugation was verified by size-exclusion chromatography as shown in Supplementary Fig. 1d, tracking polymer elution by absorbance at 214 nm through Enrich SEC 650 columns at a flow rate of 0.25 ml min$^{-1}$ in 10 mM PBS at pH 8. In the final siNP formulation, antibody-conjugated mAbCII-PEG-DB was mixed with non-functionalized PEG-DB at defined ratios (usually 1:40 conjugated to non-functionalized polymer).

**Formation of mAbCII-siNPs.** Nanoparticles (NPs) were formed by dissolving polymers in 10 mM citric acid buffer (pH 4) before complexation with siRNA for 30 min. Polymer was initially dissolved at 3 mg ml$^{-1}$ concentration. Palmitic acid-modified siRNA was complexed at an $N^+$:$P^-$ ratio of 20. Following complexation, the pH was neutralized to 7.4 with sodium phosphate buffer (10 mM, pH 8; 5:1 v/v pH 8 buffer:complexed polymer-siRNA solution in pH 4 buffer).

For in vivo experiments, siNPs were formed under the same conditions and concentrated using 50 kD MWCO 15 ml Amicon spin filters, washed with PBS, and sterile-filtered before injection.

**Characterization of siNPs.** The mAbCII-siNPs were characterized to verify that the siNP functionality was not compromised by antibody conjugation. The efficiency of siRNA encapsulation $N^+$:$P^-$ ratios was evaluated using a Quant-iT Ribogreen assay kit (ThermoFisher Scientific). siNP size was evaluated using dynamic light scattering (Zetasizer Nano ZS). Polymer pH-dependent membrane-disruptive function as a marker for endosome disruption and escape was evaluated using a haemolysis assay, as described previously[77].

**Selection of *Mmp13* siRNA.** Seven candidate siRNA sequences targeting different sites of the *Mmp13* gene were first screened in ATDC5 cells stimulated with the inflammatory cytokine TNF (20 ng ml$^{-1}$). Oligonucleotides used in these studies were purchased from Integrated DNA Technologies (Coralville) or Dharmacon. The selected sequence was synthesized with 2′-*O*-methyl modification for enhanced in vivo activity (Supplementary Table 1).

**Cell culture and viability studies.** ATDC5 cells were cultured in DMEM/F-12 GlutaMAX medium with 10% FBS, 1% penicillin-streptomycin at 37 °C in 5% $CO_2$. Relevant experiments were performed at 80% confluency. Cytotoxicity was performed using the CellTiter-Glo assay, in accordance with the manufacturer's protocol.

**Luciferase gene-silencing assay.** For in vitro luciferase knockdown assays, ATDC5 cells were transduced with lentivirus harbouring a constitutively expressed luciferase gene as previously described[36]. Cells were then seeded at 2,000 per well in clear-bottom, black-walled 96-well plates. After allowing cells to adhere for 24 h, siNPs were introduced into the medium at a concentration of 100 nM siRNA (siLUC or siNEG). Treatments were removed after 24 h of incubation, D-luciferin (150 µg ml$^{-1}$) was added to the cells, and cell bioluminescence was then measured on an IVIS Lumina III imaging system (Caliper Life Sciences) at 24 h and 48 h after treatment. Luminescence was normalized to that of siNEG NP controls. Finally, cell viability was measured by comparing luminescence of siNEG controls to untreated cells.

**Quantitative PCR.** RT–qPCR was performed utilizing TaqMan primers and reagents as outlined by the manufacturer. (ThermoFisher Scientific; GAPDH, Mm99999915_g1; ACTB, Mm02619580_g1; MMP13, Mm00439491_m1; IL6, Mm00446190_m1). *Gapdh* and *Actb* were both used to normalize *Mmp13* expression.

**In vitro matrix binding and reverse transfection in ATDC5 cells.** To select the correct polymer:antibody ratio (Fig. 2f), trypsin-damaged porcine cartilage retention was assessed. First, damaged articular cartilage 'model lesions' were created by partial trypsin damage of porcine cartilage with 2.5% trypsin for 15 min at 37 °C. Then, each plug was inserted into a well plate and treated with mAbCII-siNPs or controls. The different mAbCII-siNP formulations were tested at matched polymer and siRNA concentration in the test solutions. In the screened samples, the final antibody concentrations tested were 0.66, 1.33 and 2.66 µM for the 20:1, 40:1 and 80:1 ratios of free polymer to mAbCII-conjugated polymer. Formulations were incubated for 1 h at 37 °C followed by washing twice with PBS (200 µl each time). IVIS imaging was used to quantify retention of the rhodamine within the siNP polymer.

To test substrate-mediated delivery and potency of the mAbCII-siNPs, a reverse-transfection assay was used. Trypsin-damaged tissues (prepared as described) were incubated for 1 h with mAbCII-siNPs/siLuc, siNPs/siLuc, mAbCtrl-siNPs/siLuc, lipofectamine 2000/siLuc or the analogous formulations loaded with nonsilencing siNEG siRNA. Following incubation, explants were washed with PBS, and luciferase-expressing ATDC5 cells in DMEM/F-12 1:1 medium were seeded onto the treated cartilage for 24 h at 37 °C. In parallel samples, similar methods were used but without the wash step to help to gauge the silencing efficacy of the different formulations independent from the cartilage binding capacity. Each well was rinsed with PBS before adding luciferin-containing medium (150 µg ml$^{-1}$) and evaluating luminescence by IVIS imaging. Following measurement of luciferase expression, the cell viability of each group was determined using the Promega CellTiter-Glo cell viability assay following the manufacturer's standard protocol.

**In vivo short-term mechanical loading PTOA model.** C57 mice were mechanically loaded, three times per week for two weeks. The PTOA model of noninvasive repetitive joint loading was induced by subjecting the knee joints of mice (anaesthetized with 3% isoflurane) to 250 cycles of compressive mechanical loading at 9 N. This procedure was repeated three times per week over a period of two weeks using conditions adapted from previous studies[38,46]. All mice were obtained from Charles River Labs; the mice were male and either 8 weeks (short-term study) or 6 months (long-term study) of age. The mice were housed at Vanderbilt University's rodent housing facilities in compliance with all procedures reviewed and approved by IACUC in standard conditions (18–23 °C, 40–60% humidity, 12 h light:12 h dark cycle). All relevant IACUC animal-use guidelines and ethical regulations were followed in animal work conducted for this study.

**Joint pharmacokinetics.** In-joint retention of mAbCII-siNPs was assessed in both healthy mice and in PTOA mice using the two-week mechanical loading protocol. The normal mice and mice that had been mechanically loaded 3 times per week for 2 weeks were treated with intra-articular injection of 0.5 mg kg$^{-1}$ siRNA per knee in mAbCII-siNPs. Over the next 72 h, the amount of fluorescence remaining in the knee was measured by IVIS imaging (Living Image V4.4 software, Perkin Elmer) of the rhodamine-containing mAbCII-siNPs (Supplementary Fig. 4b; excitation/emission wavelength, 548/570 nm). Cryosections of fluorescent mAbCII-siNPs were imaged using the Nikon Czsi+ confocal microscope and analysed using Nikon NIS-Elements AR V4.30.01.

**Organ biodistribution.** Intravital imaging was performed on mice after intra-articular injection of mAbCII-siNPs (0.5 mg kg$^{-1}$ siRNA per knee) with and without mechanical induction of PTOA. These measurements were taken on the same mice used to verify mAbCII-siNP anchoring and retention within PTOA-affected knee joints (Fig. 3c) and reduced level of biodistribution to the liver relative to mice that did not have PTOA induction. These data also confirmed the anticipated result that the liver is the primary clearance organ for the siNPs (Supplementary Fig. 5a,b).

**mAbCII-siNP in vivo dose-response and longevity studies.** A progressive-dose experiment was performed with the same two-week mechanical loading model. After two weeks of mechanical loading, the joints were treated, and 72 h later joint tissues were collected for analysis of *Mmp13* and *Il1b* expression analysis by RT–qPCR (Supplementary Fig. 6a,b). A longevity-of-action study was performed by intra-articular administration of the 0.5 mg kg$^{-1}$ per knee dose of mAbCII-siNPs after two weeks of mechanical loading. Mechanical loading was continued with the same frequency to maintain elevated *Mmp13* expression in the joints, and the mice were killed at 5, 10 or 15 d after injection for gene-expression analysis (Supplementary Fig. 6c).

**In vivo long-term mechanical loading therapeutic PTOA model.** Mice were maintained to an age of 6 months and then subjected to a more rigorous cyclic mechanical loading protocol of 9 N, 500 cycles, 5 times per week for 6 weeks[47]. Doses of siRNA (0.5 mg kg$^{-1}$) were administered to each knee weekly, starting concurrently with mechanical loading. MMPSense and Alexa Fluor-labelled free mAbCII antibody were injected intravenously 24 h before the mice were euthanized to gauge total MMP activity and quantify cartilage damage, respectively.

For the clinical standard benchmarking study, a relatively high methylprednisolone dose in rodents of 4 mg kg$^{-1}$ was administered by intra-articular injection. Separate cohorts of mice were delivered either a single treatment at the beginning of the six-week time course or weekly treatment. Weekly treatment matched the mAbCII-siNP treatment protocol, while a single treatment was used to match the clinical standard, as patients are not typically treated more frequently than this with intra-articular steroid injections[78,79]. The dose was prepared by initially dissolving in DMSO, diluting in water and injecting at a volume of 20 µl per knee[74].

**Bone analysis by microCT.** All microCT analysis was performed with the ScanCo µCT-50 and ScanCo software V6.0 (Scanco). Three-dimensional renderings were shown at a consistent density threshold (42.0% of maximum bone density or 420 per mille). All samples were fixed with formalin and then submerged in 100% ethanol during microCT imaging. The scans were collected with 20-µm-thick slices, an isotropic 12 µm voxel size, a current/voltage of 114 mA/70 kVp, and an integration time of 200 ms. Imaging, contouring and all sample measurements and analyses were performed on deidentified samples by a treatment-blinded user.

**Histology and immunohistochemistry.** Stifles were fixed in 10% neutral buffered formalin and decalcified in Immunocal (StatLab). Tissue handling for histopathology was primarily performed in the Vanderbilt Translational Pathology Shared Resource (TPSR) by certified histology technicians. Fixed tissues were routinely processed using a standard 8 h cycle of graded alcohols, xylenes and paraffin wax, embedded and sectioned at 5 µm, floated on a water bath, and mounted on positively charged glass slides. H&E staining was performed on the Gemini autostainer (ThermoFisher Scientific). Safranin O staining was performed by hand using a kit (StatLab).

Stifle joints were evaluated by H&E and safranin O in at least two serial mid-frontal sections. This histopathologic interpretation was conducted by a board-certified veterinary pathologist under treatment-blinded conditions[80]. OARSI scores (0–6 semiquantitative scale) were provided for the medial tibial plateau and lateral tibial plateau[50]. Simultaneously, a generic score (0–4 semiquantitative scale) was assigned based on safranin O staining of the tibial plateau (Supplementary Table 2a) and on H&E features of DJD severity, as defined by cartilage degeneration, meniscal metaplasia, subchondral osteosclerosis, synovial hyperplasia and inflammation and osteophyte/meniscal mineral deposit formation[81] (Supplementary Table 2b).

Immunohistochemical staining was performed on a Leica Bond-Max autostainer (Leica Biosystems). All steps besides dehydration, clearing and

coverslipping were performed on the Bond-Max where all the slides were deparaffinized. Heat-induced antigen retrieval was performed on the Bond-Max using Epitope Retrieval 1 solution (Leica Biosystems) for 20 min. Slides were incubated with anti-MMP13 (Abcam Ab39012) for 1 h at a 1:750 dilution. The Bond Polymer Refine detection system (Leica Biosystems) was used for visualization. Slides were then dehydrated, cleared and coverslipped.

**nanoString inflammation panel gene-expression analysis.** The Vanderbilt Technologies for Advanced Genomics (VANTAGE) core processed the RNA (>50 ng purified, normalized RNA per sample) isolated from articular cartilage and meniscal/synovial tissue processed in equal masses. Samples were subjected to VANTAGE core quality control measures before processing using the nanoString nCounter Inflammation (mouse, v2) panel. All hybridizations were incubated for 20 h, following the manufacturer's (Nanostring Technologies) recommended procedures. The nSolver V3.0 software package (Nanostring Technologies) was used for comparisons, unsupervised analysis, and gene-cluster analysis between groups. Raw and normalized data are available in Gene Expression Omnibus under accession GSE171031.

**Statistical analysis.** All statistical analysis was performed as described in figure captions with GraphPad Prism V8.2 (GraphPad), except for nanoString data analysis with nSolver V3.0 (Nanostring Technologies).

**Reporting summary.** Further information on research design is available in the Nature Research Reporting Summary linked to this article.

## Data availability

The main data supporting the results in this study are available within the paper and its Supplementary Information. Raw and normalized nanoString datasets are available at the Gene Expression Omnibus under accession identifier GSE171031. The remaining raw and analysed datasets from the study are too large to be publicly shared, but they are available for research purposes from the corresponding author on reasonable request.

Received: 18 April 2019; Accepted: 10 July 2021;
Published online: 19 August 2021

## References

1. Loeser, R. F. Osteoarthritis year in review 2013: biology. *Osteoarthr. Cartil.* **21**, 1436–1442 (2013).
2. Tanamas, S. et al. Does knee malalignment increase the risk of development and progression of knee osteoarthritis? A systematic review. *Arthritis Care Res.* **61**, 459–467 (2009).
3. Richette, P. et al. Benefits of massive weight loss on symptoms, systemic inflammation and cartilage turnover in obese patients with knee osteoarthritis. *Ann. Rheum. Dis.* **70**, 139–144 (2011).
4. Valdes, A. M. & Spector, T. D. Genetic epidemiology of hip and knee osteoarthritis. *Nat. Rev. Rheumatol.* **7**, 23–32 (2011).
5. Issa, S. & Sharma, L. Epidemiology of osteoarthritis: an update. *Curr. Rheumatol. Rep.* **8**, 7–15 (2006).
6. Lee, A. S. et al. A current review of molecular mechanisms regarding osteoarthritis and pain. *Gene* **527**, 440–447 (2013).
7. Zhang, Y. & Jordan, J. M. Epidemiology of osteoarthritis. *Clin. Geriatr. Med.* **26**, 355–369 (2010).
8. Brophy, R. H., Gray, B. L., Nunley, R. M., Barrack, R. L. & Clohisy, J. C. Total knee arthroplasty after previous knee surgery. *J. Bone Jt. Surg. Am.* **96A**, 801–805 (2014).
9. Brown, T. D., Johnston, R. C., Saltzman, C. L., Marsh, J. L. & Buckwalter, J. A. Posttraumatic osteoarthritis: a first estimate of incidence, prevalence, and burden of disease. *J. Orthop. Trauma* **20**, 739–744 (2006).
10. Young, I. C. et al. A novel compressive stress-based osteoarthritis-like chondrocyte system. *Exp. Biol. Med.* **242**, 1062–1071 (2017).
11. Martin, J. & Buckwalter, J. Post-traumatic osteoarthritis: the role of stress induced chondrocyte damage. *Biorheology* **43**, 517–521 (2006).
12. McAlindon, T. E. et al. OARSI guidelines for the non-surgical management of knee osteoarthritis. *Osteoarthr. Cartil.* **22**, 363–388 (2014).
13. McAlindon, T. E. et al. Effect of intra-articular triamcinolone vs saline on knee cartilage volume and pain in patients with knee osteoarthritis: a randomized clinical trial. *JAMA* **317**, 1967–1975 (2017).
14. Wijn, S. R. W., Rovers, M. M., van Tienen, T. G. & Hannink, G. Intra-articular corticosteroid injections increase the risk of requiring knee arthroplasty. *Bone Jt. J.* **102-B**, 586–592 (2020).
15. Wernecke, C., Braun, H. J. & Dragoo, J. L. The effect of intra-articular corticosteroids on articular cartilage: a systematic review. *Orthop. J. Sports Med.* **3**, 2325967115581163 (2015).
16. Wang, M. et al. MMP13 is a critical target gene during the progression of osteoarthritis. *Arthritis Res. Ther.* **15**, R5 (2013).
17. Krzeski, P. et al. Development of musculoskeletal toxicity without clear benefit after administration of PG-116800, a matrix metalloproteinase inhibitor, to patients with knee osteoarthritis: a randomized, 12-month, double-blind, placebo-controlled study. *Arthritis Res. Ther.* **9**, R109 (2007).
18. Molina, J. R. et al. A phase I and pharmacokinetic study of the selective, non-peptidic inhibitor of matrix metalloproteinase BAY 12-9566 in combination with etoposide and carboplatin. *Anticancer Drugs* **16**, 997–1002 (2005).
19. Clutterbuck, A. L., Asplin, K. E., Harris, P., Allaway, D. & Mobasheri, A. Targeting matrix metalloproteinases in inflammatory conditions. *Curr. Drug Targets* **10**, 1245–1254 (2009).
20. Liu, J. & Khalil, R. A. Matrix metalloproteinase inhibitors as investigational and therapeutic tools in unrestrained tissue remodeling and pathological disorders. *Prog. Mol. Biol. Transl. Sci.* **148**, 355–420 (2017).
21. Settle, S. et al. Cartilage degradation biomarkers predict efficacy of a novel, highly selective matrix metalloproteinase 13 inhibitor in a dog model of osteoarthritis: confirmation by multivariate analysis that modulation of type II collagen and aggrecan degradation peptides parallels pathologic changes. *Arthritis Rheum.* **62**, 3006–3015 (2010).
22. Cai, H. et al. Assessment of the renal toxicity of novel anti-inflammatory compounds using cynomolgus monkey and human kidney cells. *Toxicology* **258**, 56–63 (2009).
23. Sterner, B. et al. The effect of polymer size and charge of molecules on permeation through synovial membrane and accumulation in hyaline articular cartilage. *Eur. J. Pharm. Biopharm.* **101**, 126–136 (2016).
24. Larsen, C. et al. Intra-articular depot formulation principles: role in the management of postoperative pain and arthritic disorders. *J. Pharm. Sci.* **97**, 4622–4654 (2008).
25. Evans, C. H., Kraus, V. B. & Setton, L. A. Progress in intra-articular therapy. *Nat. Rev. Rheumatol.* **10**, 11–22 (2013).
26. Simkin, P. A. Synovial perfusion and synovial fluid solutes. *Ann. Rheum. Dis.* **54**, 424–428 (1995).
27. Rothenfluh, D. A., Bermudez, H., O'Neil, C. P. & Hubbell, J. A. Biofunctional polymer nanoparticles for intra-articular targeting and retention in cartilage. *Nat. Mater.* **7**, 248–254 (2008).
28. Zhou, F. et al. Silk fibroin-chondroitin sulfate scaffold with immuno-inhibition property for articular cartilage repair. *Acta Biomater.* **63**, 64–75 (2017).
29. Hayder, M. et al. A phosphorus-based dendrimer targets inflammation and osteoclastogenesis in experimental arthritis. *Sci. Transl. Med.* **3**, 81ra35 (2011).
30. Chen, K. & Chen, X. Integrin targeted delivery of chemotherapeutics. *Theranostics* **1**, 189–200 (2011).
31. Hoy, S. M. Patisiran: first global approval. *Drugs* **78**, 1625–1631 (2018).
32. de Paula Brandão, P. R., Titze-de-Almeida, S. S. & Titze-de-Almeida, R. Leading RNA interference therapeutics part 2: silencing delta-aminolevulinic acid synthase 1, with a focus on givosiran. *Mol. Diagnosis Ther.* **24**, 61–68 (2019).
33. Nelson, C. E. et al. Balancing cationic and hydrophobic content of PEGylated siRNA polyplexes enhances endosome escape, stability, blood circulation time, and bioactivity in vivo. *ACS Nano* **7**, 8870–8880 (2013).
34. Beavers, K. R., Nelson, C. E. & Duvall, C. L. MiRNA inhibition in tissue engineering and regenerative medicine. *Adv. Drug Deliv. Rev.* **88**, 123–137 (2015).
35. Sarett, S. M. et al. Hydrophobic interactions between polymeric carrier and palmitic acid-conjugated siRNA improve PEGylated polyplex stability and enhance in vivo pharmacokinetics and tumor gene silencing. *Biomaterials* **97**, 122–132 (2016).
36. Jackson, M. A. et al. Zwitterionic nanocarrier surface chemistry improves siRNA tumor delivery and silencing activity relative to polyethylene glycol. *ACS Nano* **11**, 5680–5696 (2017).
37. Ruan, M. Z. et al. Proteoglycan 4 expression protects against the development of osteoarthritis. *Sci. Transl. Med.* **5**, 176ra134 (2013).
38. Cho, H., Pinkhassik, E., David, V., Stuart, J. M. & Hasty, K. A. Detection of early cartilage damage using targeted nanosomes in a post-traumatic osteoarthritis mouse model. *Nanomed. Nanotechnol. Biol. Med.* **11**, 939–946 (2015).
39. Werfel, T. A. et al. Selective mTORC2 inhibitor therapeutically blocks breast cancer cell growth and survival. *Cancer Res.* **78**, 1845–1858 (2018).
40. Werfel, T. A. et al. Combinatorial optimization of PEG architecture and hydrophobic content improves ternary siRNA polyplex stability, pharmacokinetics, and potency in vivo. *J. Control. Release* **255**, 12–26 (2017).
41. Kilchrist, K. V. et al. Gal8 visualization of endosome disruption predicts carrier-mediated biologic drug intracellular bioavailability. *ACS Nano* **13**, 1136–1152 (2019).
42. Jackson, M. A. et al. Dual carrier–cargo hydrophobization and charge ratio optimization improve the systemic circulation and safety of zwitterionic nano-polyplexes. *Biomaterials* **192**, 245–259 (2019).

43. Griffin, D. J. et al. Effects of enzymatic treatments on the depth-dependent viscoelastic shear properties of articular cartilage. *J. Orthop. Res.* **32**, 1652–1657 (2014).
44. Cho, H. et al. Theranostic immunoliposomes for osteoarthritis. *Nanomedicine* **10**, 619–627 (2014).
45. Jasin, H. E., Noyori, K., Takagi, T. & Taurog, J. D. Characteristics of anti-type II collagen antibody binding to articular cartilage. *Arthritis Rheum.* **36**, 651–659 (1993).
46. Poulet, B., Hamilton, R. W., Shefelbine, S. & Pitsillides, A. A. Characterizing a novel and adjustable noninvasive murine joint loading model. *Arthritis Rheum.* **63**, 137–147 (2011).
47. Ko, F. C. et al. In vivo cyclic compression causes cartilage degeneration and subchondral bone changes in mouse tibiae. *Arthritis Rheum.* **65**, 1569–1578 (2013).
48. Scanzello, C. R. & Goldring, S. R. The role of synovitis in osteoarthritis pathogenesis. *Bone* **51**, 249–257 (2012).
49. Goldring, M. B. Articular cartilage degradation in osteoarthritis. *HSS J.* **8**, 7–9 (2012).
50. Glasson, S. S., Chambers, M. G., Van Den Berg, W. B. & Little, C. B. The OARSI histopathology initiative—recommendations for histological assessments of osteoarthritis in the mouse. *Osteoarthr. Cartil.* **18**, S17–S23 (2010).
51. Eichaker, L. R., Cho, H., Duvall, C. L., Werfel, T. A. & Hasty, K. A. Future nanomedicine for the diagnosis and treatment of osteoarthritis. *Nanomedicine* **9**, 2203–2215 (2014).
52. O'Grady, K. P. et al. Drug-free ROS sponge polymeric microspheres reduce tissue damage from ischemic and mechanical injury. *ACS Biomater. Sci. Eng.* **4**, 1251–1264 (2017).
53. Sun, Y. & Mauerhan, D. R. Meniscal calcification, pathogenesis and implications. *Curr. Opin. Rheumatol.* **24**, 152–157 (2012).
54. Blom, A. B. et al. Crucial role of macrophages in matrix metalloproteinase-mediated cartilage destruction during experimental osteoarthritis: involvement of matrix metalloproteinase 3. *Arthritis Rheum.* **56**, 147–157 (2007).
55. Hügle, T. & Geurts, J. What drives osteoarthritis?—Synovial versus subchondral bone pathology. *Rheumatology* **56**, 1461–1471 (2016).
56. Goldring, S. R. Alterations in periarticular bone and cross talk between subchondral bone and articular cartilage in osteoarthritis. *Ther. Adv. Musculoskelet. Dis.* **4**, 249–258 (2012).
57. Boileau, C., Tat, S. K., Pelletier, J. P., Cheng, S. & Martel-Pelletier, J. Diacerein inhibits the synthesis of resorptive enzymes and reduces osteoclastic differentiation/survival in osteoarthritic subchondral bone: a possible mechanism for a protective effect against subchondral bone remodelling. *Arthritis Res. Ther.* **10**, R71 (2008).
58. Punzi, L. et al. Post-traumatic arthritis: overview on pathogenic mechanisms and role of inflammation. *RMD Open* **2**, e000279 (2016).
59. Christiansen, B. A. et al. Non-invasive mouse models of post-traumatic osteoarthritis. *Osteoarthr. Cartil.* **23**, 1627–1638 (2015).
60. Almasry, S. M., Soliman, H. M., El-Tarhouny, S. A., Algaidi, S. A. & Ragab, E. M. Platelet rich plasma enhances the immunohistochemical expression of platelet derived growth factor and vascular endothelial growth factor in the synovium of the meniscectomized rat models of osteoarthritis. *Ann. Anat.* **197**, 38–49 (2015).
61. Solomon, L. A., Bérubé, N. G. & Beier, F. Transcriptional regulators of chondrocyte hypertrophy. *Birth Defects Res. C* **84**, 123–130 (2008).
62. Zhai, G., Doré, J. & Rahman, P. TGF-β signal transduction pathways and osteoarthritis. *Rheumatol. Int.* **35**, 1283–1292 (2015).
63. Shen, J., Li, S. & Chen, D. TGF-β signaling and the development of osteoarthritis. *Bone Res.* https://doi.org/10.1038/boneres.2014.2 (2014).
64. Lee, Y. H. et al. Enzyme-crosslinked gene-activated matrix for the induction of mesenchymal stem cells in osteochondral tissue regeneration. *Acta Biomater.* **63**, 210–226 (2017).
65. John, T., Stahel, P. F., Morgan, S. J. & Schulze-Tanzil, G. Impact of the complement cascade on posttraumatic cartilage inflammation and degradation. *Histol. Histopathol.* **22**, 781–790 (2007).
66. Silawal, S., Triebel, J., Bertsch, T. & Schulze-Tanzil, G. Osteoarthritis and the complement cascade. *Clin. Med. Insights Arthritis Musculoskelet. Disord.* **11**, 1179544117751430 (2018).
67. Lubbers, R., van Essen, M. F., van Kooten, C. & Trouw, L. A. Production of complement components by cells of the immune system. *Clin. Exp. Immunol.* **188**, 183–194 (2017).
68. Takahashi, N. et al. Elucidation of IL-1/TGF-β interactions in mouse chondrocyte cell line by genome-wide gene expression. *Osteoarthr. Cartil.* **13**, 426–438 (2005).
69. Klein-Wieringa, I. R. et al. Inflammatory cells in patients with endstage knee osteoarthritis: a comparison between the synovium and the infrapatellar fat pad. *J. Rheumatol.* **43**, 771–778 (2016).
70. Wu, C. L., Harasymowicz, N. S., Klimak, M. A., Collins, K. H. & Guilak, F. The role of macrophages in osteoarthritis and cartilage repair. *Osteoarthr. Cartil.* https://doi.org/10.1016/j.joca.2019.12.007 (2020).
71. Mazur, C. M. et al. Osteocyte dysfunction promotes osteoarthritis through MMP13-dependent suppression of subchondral bone homeostasis. *Bone Res.* **7**, 34 (2019).
72. Goldring, S. R. & Goldring, M. B. in *Kelley's Textbook of Rheumatology* 1–19.e16 (Elsevier, 2017).
73. Garg, N., Perry, L. & Deodhar, A. Intra-articular and soft tissue injections, a systematic review of relative efficacy of various corticosteroids. *Clin. Rheumatol.* **33**, 1695–1706 (2014).
74. Cho, H., Walker, A., Williams, J. & Hasty, K. A. Study of osteoarthritis treatment with anti-inflammatory drugs: cyclooxygenase-2 inhibitor and steroids. *BioMed. Res. Int.* **2015**, 595273 (2015).
75. Hoshyar, N., Gray, S., Han, H. & Bao, G. The effect of nanoparticle size on in vivo pharmacokinetics and cellular interaction. *Nanomed.* **11**, 673–692 (2016).
76. Terato, K. et al. Induction of arthritis with monoclonal antibodies to collagen. *J. Immunol.* **148**, 2103–2108 (1992).
77. Evans, B. C. et al. Ex vivo red blood cell hemolysis assay for the evaluation of pH-responsive endosomolytic agents for cytosolic delivery of biomacromolecular drugs. *J. Vis. Exp.* **73**, e50166 (2013).
78. Polderman, J. A. et al. Adverse side effects of dexamethasone in surgical patients. *Cochrane Database Syst. Rev.* **11**, CD011940 (2018).
79. Orak, M. M. et al. Comparison of the effects of chronic intra-articular administration of tenoxicam, diclofenac, and methylprednisolone in healthy rats. *Acta Orthop. Traumatol. Turc.* **49**, 438–446 (2015).
80. Bolon, B. et al. Rodent preclinical models for developing novel antiarthritic molecules: comparative biology and preferred methods for evaluating efficacy. *J. Biomed. Biotechnol.* **2011**, 569068 (2011).
81. Aigner, T. & Söder, S. Histopathologische Begutachtung der Gelenkdegeneration. *Der. Pathol.* **27**, 431–438 (2006).


## Acknowledgements

The authors acknowledge the assistance of the Vanderbilt TPSR. The TPSR is supported by National Cancer Institute/National Insitutes for Health (NIH) Cancer Center Support Grant 2P30 CA068485-14. Dynamic light scattering was conducted at the Vanderbilt Institute of Nanoscale Sciences and Engineering. Bone analysis by microCT was supported in part by the NIH (S10RR027631-01). We thank C. B. Wiese, J. R. Johnson and R. Mernaugh for technical assistance. The VANTAGE core performed nanoString QC and hybridization, and is supported by the Vanderbilt Ingram Cancer Center (P30 CA68485), the Vanderbilt Vision Center (P30 EY08126) and NIH/National Centre for Research Resources (G20 RR030956). We thank the Department of Defense (DOD CDMRP OR130302), NIH (NIH R01 CA224241 and NIH R01 EB019409), NIH (NIGMS T32GM007347), the Veterans Association Merit Award BX004151, the National Science Foundation Graduate Research Fellowship Program (NSF GRF 2016212929), the Natural Sciences and Engineering Research Council of Canada (NSERC) and the Rheumatology Research Foundation (RRF) for support.

## Author contributions

S.K.B., C.L.D., K.A.H., L.J.C. and J.M.C. designed the project and experiments. S.K.B. synthesized the polymers and conjugates and formulated nanoparticles for all experiments. S.K.B. and F.Y. conducted all animal experiments. S.K.B., M.A.J. and D.D.L. performed nanoparticle characterization. S.K.B., F.Y., J.M.C. and D.D.L. imaged and collected tissues. L.E.H. and H.C. conducted histology and immunohistochemistry, with L.E.H. performing blinded scoring of histology. S.K.B., C.L.D. and J.M.C. wrote the manuscript. All authors reviewed and commented on the manuscript.

## Competing interests

The authors declare no competing interests.

## Additional information

**Supplementary information** The online version contains supplementary material available at https://doi.org/10.1038/s41551-021-00780-3.

**Correspondence and requests for materials** should be addressed to C.L.D.

**Peer review information** *Nature Biomedical Engineering* thanks Fergal O'Brien, Ahuva Nissim and the other, anonymous, reviewer(s) for their contribution to the peer review of this work.

**Reprints and permissions information** is available at www.nature.com/reprints.

**Publisher's note** Springer Nature remains neutral with regard to jurisdictional claims in published maps and institutional affiliations.

nature research

Corresponding author(s): Craig Duvall

Last updated by author(s): Apr 10, 2021

# Reporting Summary

Nature Research wishes to improve the reproducibility of the work that we publish. This form provides structure for consistency and transparency in reporting. For further information on Nature Research policies, see Authors & Referees and the Editorial Policy Checklist.

## Statistics

For all statistical analyses, confirm that the following items are present in the figure legend, table legend, main text, or Methods section.

| n/a | Confirmed |
|---|---|
| ☐ | ☒ The exact sample size (*n*) for each experimental group/condition, given as a discrete number and unit of measurement |
| ☐ | ☒ A statement on whether measurements were taken from distinct samples or whether the same sample was measured repeatedly |
| ☐ | ☒ The statistical test(s) used AND whether they are one- or two-sided<br>*Only common tests should be described solely by name; describe more complex techniques in the Methods section.* |
| ☒ | ☐ A description of all covariates tested |
| ☐ | ☒ A description of any assumptions or corrections, such as tests of normality and adjustment for multiple comparisons |
| ☐ | ☒ A full description of the statistical parameters including central tendency (e.g. means) or other basic estimates (e.g. regression coefficient) AND variation (e.g. standard deviation) or associated estimates of uncertainty (e.g. confidence intervals) |
| ☐ | ☒ For null hypothesis testing, the test statistic (e.g. *F*, *t*, *r*) with confidence intervals, effect sizes, degrees of freedom and *P* value noted<br>*Give P values as exact values whenever suitable.* |
| ☒ | ☐ For Bayesian analysis, information on the choice of priors and Markov chain Monte Carlo settings |
| ☒ | ☐ For hierarchical and complex designs, identification of the appropriate level for tests and full reporting of outcomes |
| ☒ | ☐ Estimates of effect sizes (e.g. Cohen's *d*, Pearson's *r*), indicating how they were calculated |

*Our web collection on statistics for biologists contains articles on many of the points above.*

## Software and code

Policy information about availability of computer code

| | |
|---|---|
| Data collection | Living Image IVIS Software V4.4. |
| Data analysis | Graphpad Prism V8.2, Nikon NIS-Elements AR V4.30.01, Microsoft Excel 2013, SCANCO Medical microCT software suite V6.0, and nSolver V3.0. |

For manuscripts utilizing custom algorithms or software that are central to the research but not yet described in published literature, software must be made available to editors/reviewers. We strongly encourage code deposition in a community repository (e.g. GitHub). See the Nature Research guidelines for submitting code & software for further information.

## Data

Policy information about availability of data

All manuscripts must include a data availability statement. This statement should provide the following information, where applicable:

- Accession codes, unique identifiers, or web links for publicly available datasets
- A list of figures that have associated raw data
- A description of any restrictions on data availability

The main data supporting the results in this study are available within the paper and its Supplementary Information. Raw and normalized nanoString datasets are available within the Gene Expression Omnibus with the accession identifier GSE171031 (https://www.ncbi.nlm.nih.gov/geo/query/acc.cgi?acc=GSE171031). The remaining raw and analysed datasets from the study are too large to be publicly shared, yet they are available for research purposes from the corresponding author on reasonable request.

# Field-specific reporting

Please select the one below that is the best fit for your research. If you are not sure, read the appropriate sections before making your selection.

☒ Life sciences ☐ Behavioural & social sciences ☐ Ecological, evolutionary & environmental sciences

For a reference copy of the document with all sections, see nature.com/documents/nr-reporting-summary-flat.pdf

# Life sciences study design

All studies must disclose on these points even when the disclosure is negative.

| | |
|---|---|
| Sample size | In vitro studies were performed with at least 3 technical replicates. In the process of piloting the mechanical-overload osteoarthritis model, the differences between mice subjected to the model and healthy mice were used to educate a power analysis for sample-size selection. Not all intra-articular injections were successfully administered, resulting in some reported variation in sample size between the in vivo treatment groups. |
| Data exclusions | No data were excluded from the analyses. |
| Replication | All in vitro experiments were performed with at least three technical replicates on more than one occasion to ensure reproducibility across experiments, and all in vivo experiments were performed with sufficient technical replicates to ensure reproducibility. All in vivo studies were done in one cohort, with the indicated sample sizes. The completion of two large in vivo studies in a short-term model and a long-term model and the consistency of the gene-silencing results between these two studies supports their reproducibility. All internal attempts at replication were successful. |
| Randomization | For the in vivo studies, the animals were randomly assigned to treatment groups at the outset of the study. In the short-term model, mice were assigned consecutive numbers across cages, and the groups were clustered consecutive numbers at random. In the long-term model, animals were assigned to groups interspersed at random between cages for the most variety within each cage throughout the study. All animals were age-matched, with no observed differences or selection criteria for a specific treatment group. |
| Blinding | The researcher who performed the mechanical joint loading and intra-articular injections was not involved in the preparation of the injected treatments and was not involved in the design of the study groups. The histopathologist who completed the scoring of OA severity by the DJD and OARSI metrics was blinded to the treatment given to the animals and was also not involved in the overall design of the study. |

# Reporting for specific materials, systems and methods

We require information from authors about some types of materials, experimental systems and methods used in many studies. Here, indicate whether each material, system or method listed is relevant to your study. If you are not sure if a list item applies to your research, read the appropriate section before selecting a response.

## Materials & experimental systems

| n/a | Involved in the study |
|---|---|
| ☐ | ☒ Antibodies |
| ☐ | ☒ Eukaryotic cell lines |
| ☒ | ☐ Palaeontology |
| ☐ | ☒ Animals and other organisms |
| ☒ | ☐ Human research participants |
| ☒ | ☐ Clinical data |

## Methods

| n/a | Involved in the study |
|---|---|
| ☒ | ☐ ChIP-seq |
| ☒ | ☐ Flow cytometry |
| ☒ | ☐ MRI-based neuroimaging |

## Antibodies

| | |
|---|---|
| Antibodies used | Anti-MMP13 antibody (ab39012), Abcam, Cambridge, MA.<br>We produced a murine igG-2c monoclonal antibody targeting collagen-II from a hybridoma. |
| Validation | For immunohistochemical staining for MMP13, slides were incubated with anti-MMP13 antibody for 1 hour at a 1:750 dilution. The antibody was validated by the commercial supplier for human species, and has been validated in multiple species in published studies, including mice (citation: Tsubosaka M et al. Gelatin hydrogels with eicosapentaenoic acid can prevent osteoarthritis progression in vivo in a mouse model. J Orthop Res N/A:N/A (2020)). The supplier confirms the reactivity of certain forms of MMP13 in the following statement: "ab39012 recognizes the latent proenzyme, at 60 Kd, as well as the active form at 48 Kd, and intermediate activation forms. It does not cross react with the other MMP family members. ab39012 recognizes the Hinge region of MMP13".<br><br>Characterization and validation of the murine igG-2c monoclonal antibody for collagen-II binding across species, including mice, spans several publications (included below). Cross-species reactivity is further demonstrated in murine, porcine, human and bovine tissues in the Supplementary Information. |

Noyori K, Koshino T, Takagi T, Okamoto R, Jasin HE. Binding characteristics of antitype II collagen antibody to the surface of diseased human cartilage as a probe for tissue damage. J Rheumatol. 1994;21(2):293-6. PubMed PMID: 8182639.

Jasin HE, Noyori K, Takagi T, Taurog JD. Characteristics of anti-type II collagen antibody binding to articular cartilage. Arthritis Rheum. 1993;36(5):651-9. doi: 10.1002/art.1780360512. PubMed PMID: 8489543.

Eichaker LR, Cho H, Duvall CL, Werfel TA, Hasty KA. Future nanomedicine for the diagnosis and treatment of osteoarthritis. Nanomedicine. 2014;9(14):2203-15. doi: 10.2217/nnm.14.138. PubMed PMID: WOS:000345285700012.

## Eukaryotic cell lines

Policy information about cell lines

| | |
|---|---|
| Cell line source(s) | ATDC5 (ECACC 99072806) cells (Millipore Sigma Inc., Burlington, MA). Cells were validated and maintained according to the instructions of the supplier:<br><br>Culture Medium: DMEM: Ham's F12 (1:1) + 2mM Glutamine + 5% Foetal Bovine Serum (FBS).<br><br>Subculture routine: Split sub-confluent cultures (70-80%) i.e. seeding at 1-3 x 10,000 cells/cm² using 0.25% trypsin or trypsin/EDTA; CO2; 37°C subculture every 2–3 days. |
| Authentication | Cells were authenticated according to the standards of the European Collection of Authenticated Cell Cultures, and cultured within the advised passage limits. |
| Mycoplasma contamination | All cells tested negative for mycoplasma, and were expanded in media containing a mycoplasma prophylactic (plasmocin). |
| Commonly misidentified lines (See ICLAC register) | No commonly misidentified cell lines were used. |

## Animals and other organisms

Policy information about studies involving animals; ARRIVE guidelines recommended for reporting animal research

| | |
|---|---|
| Laboratory animals | c57bl/6 mice were sourced from Charles River Labs (Wilmington, MA). |
| Wild animals | The study did not involve wild animals. |
| Field-collected samples | The study did not involve samples collected from the field. |
| Ethics oversight | All animal studies were performed in accordance with protocols reviewed and approved by the Vanderbilt University IACUC Office. |

Note that full information on the approval of the study protocol must also be provided in the manuscript.